Earth and Planetary Science Letters 288 (2009) 44–57

Contents lists available at ScienceDirect

Earth and Planetary Science Letters

journal homepage: www.elsevier.com/locate/epsl

Ultra-primitive interplanetary dust particles from the comet 26P/Grigg–Skjellerup dust stream collection

Henner Busemann [a,*], Ann N. Nguyen [a], George D. Cody [b], Peter Hoppe [c], A.L. David Kilcoyne [d], Rhonda M. Stroud [e], Thomas J. Zega [e], Larry R. Nittler [a]

[a] Department of Terrestrial Magnetism, Carnegie Institution of Washington, 5241 Broad Branch Road, NW, Washington, DC 20015, USA
[b] Geophysical Laboratory, Carnegie Institution of Washington, 5251 Broad Branch Road, NW, Washington, DC 20015, USA
[c] Particle Chemistry, Max Planck Institute for Chemistry, P.O. Box 3060, D-55020 Mainz, Germany
[d] Advanced Light Source, Lawrence Berkeley National Laboratory, Berkeley, California 94720, USA
[e] Materials Science and Technology Division, U.S. Naval Research Laboratory, Washington DC 20375, USA

ARTICLE INFO

Article history:
Received 2 June 2009
Received in revised form 2 September 2009
Accepted 4 September 2009
Available online 8 October 2009

Editor: T. Spohn

Keywords:
interplanetary dust particles
comet Grigg–Skjellerup
interstellar medium
organic matter
solar system formation
presolar grains

ABSTRACT

Cometary material and pristine interplanetary dust particles (IDPs) best resemble the unaltered components from which our solar system was built because they have remained largely unaltered in a cold undisturbed environment since accretion in the outer protoplanetary disk. IDPs might supply more primitive assemblages for laboratory analysis than Stardust samples from comet 81P/Wild 2 but their individual provenances are typically unknown. We speculate that some IDPs collected by NASA in April 2003 may be associated with comet 26P/Grigg–Skjellerup because their particularly pristine character coincides with the collection period that was predicted to show an enhanced flux of particles from this Jupiter-family comet. Some IDPs from this collection contain the most primitive assembly of interstellar matter found to date including an unusually high abundance of presolar grains and very isotopically anomalous and disordered organic matter as well as fine-grained carbonates and an amphibole associated with a GEMS-like object (glass with embedded metals and sulfides) that potentially imply formation in a nebular rather than planetary environment. The two most primitive IDPs may contain assemblages of molecular cloud material at the percent level which is supported by the presence of four rare ^{17}O-depleted presolar silicate grains possibly of supernova(e) origin within one ~70 μm^2-sized IDP and the close association of a Group 1 Mg-rich olivine from a low-mass red giant star with a carbonaceous nano-globule of potentially interstellar origin. Our study together with observations of comet 9P/Tempel 1 during the Deep Impact experiment and 81P/Wild 2 dust analyses reveal some compositional variations and many similarities among three Jupiter-family comets. Specifically carbonates and primitive organic matter or amorphous carbon were widespread in the comet-forming regions of the outer protoplanetary disk and not all comets contain as much inner solar system material as has been inferred for comet 81P/Wild 2. The bulk and hotspot hydrogen and nitrogen isotopic anomalies as well as the carbon Raman characteristics of the organic matter in IDPs and the most primitive meteorites are remarkably similar. This implies that the same mixture of molecular cloud material had been transported inward into the meteorite-forming regions of the solar system.

1. Introduction

Understanding the evolution of our solar system from the protosolar cloud of dust and gas to its present state requires analysis of the most primitive materials available, i.e., matter that was not severely altered by thermal or aqueous processing either in the solar nebula or on planetary bodies. Comets are thought to best preserve the most pristine materials because they spend most—or all—of their lifetime in the colder outer regions of the solar system (Alexander et al., 2007b; Charnley and Rodgers, 2008a; Wooden, 2008). Many interplanetary dust particles (IDPs) collected in the stratosphere show highly primitive characteristics testifying to their origin in comets (Brownlee et al., 1995; Bradley, 2003) or pristine planetary bodies in the asteroid belt not sampled by known meteorite classes. Only the most unaltered meteorites have comparably primitive properties (e.g., extreme isotope anomalies associated with organic matter, and high presolar grain abundances) to those found in many IDPs. Hence, IDPs are the most relevant reference materials available for comparison with the dust from Jupiter-family comet (JFC) 81P/Wild 2 that

* Corresponding author. School of Earth, Atmospheric and Environmental Sciences, The University of Manchester, Williamson Building, Oxford Road, Manchester M13 9PL, UK. Tel.: +44 161 275 07 69; fax: +44 161 306 93 61.
E-mail address: henner.busemann@manchester.ac.uk (H. Busemann).

0012-821X/$ – see front matter © 2009 Elsevier B.V. All rights reserved.
doi:10.1016/j.epsl.2009.09.007

was returned to Earth by NASA's Stardust mission and found to contain surprisingly large amounts of processed material (Brownlee et al., 2006; Ishii et al., 2008).

In contrast to Stardust samples, the specific parent bodies of IDPs are in general unknown. However, calculations (Messenger, 2002) predicted that 1 to 50% of the total flux of IDPs >40 μm in diameter collected after Earth passed through comet Grigg–Skjellerup's dust stream in April 2003 would originate from this comet. We analyzed several IDPs from NASA's dedicated "Grigg–Skjellerup collection" (GSC, Table 1) and compared them to Wild 2 dust, primitive meteorites and IDPs not associated with a specific dust stream. Four collectors (L2054, L2055, U2120, and U2121) were exclusively exposed for 7.9 h between April 30 and May 1, 2003 to the interplanetary dust stream thought to be enriched in dust from comet Grigg–Skjellerup (see http://www-curator.jsc.nasa.gov/dust/Leonid_shwr_Grigg_Skjellerup.cfm). The comet, probably first observed in 1808 by J. L. Pons (Kresák, 1987) and officially "discovered" in 1902 and 1922 by J. Grigg and J. F. Skjellerup, has an average orbital period of 4.98 yr (at present 5.31 yr). In 2003, the comet completed its 39th revolution since 1908 with perihelion at 0.75 to 1.12 AU. For comparison, Wild 2 showed a perihelion of 4.95 AU before 1974 and of ~1.5 AU since closely encountering Jupiter (present orbital period ~6.17 yr, 5 rev until 2004 with the close orbit around the Sun).

2. Experimental

2.1. Sample preparation

All IDP samples were transferred from NASA glass slides (free from silicone oil that is used for collection) with a Narishige MMN-1/MMO-202D micromanipulator system and commercial W micro-needles with sharpened tips of ≤1 μm diameter. The IDPs were pressed into cleaned and annealed high-purity gold foils placed on Al stubs to allow high conductivity for secondary ion mass spectrometry with reduced sample charging and focused imaging of the entire particles.

2.2. Scanning electron microscopy (SEM)

Electron images (Figs. 1 and S1) and energy dispersive spectrometry (EDS) X-ray analyses were obtained, prior to SIMS analysis, with the Carnegie Institution JEOL JSM6500F FE-SEM. An accelerating voltage of 10 keV and rapid acquisition were used to prevent beam damage and C contamination. X-ray spectra show the roughly chondritic composition of the IDPs.

2.3. Secondary ion mass spectrometry (SIMS)

The analyses were performed with Cameca ims-6f and NanoSIMS 50 L ion microprobes at the Carnegie Institution of Washington (CIW) and the NanoSIMS 50 at MPI Mainz (Hoppe et al., 2004). All measurements were made in scanning imaging mode, where the primary Cs^+ beam is rastered over the sample and secondary ions are synchronously collected in up to seven (CIW) or five (Mainz) electron multiplier detectors (6f: one multiplier, peak jumping mode), resulting in 256×256 or 512×512 pixel images. Data were reduced using the L'Image software package (L. R. Nittler, Carnegie Institution). Due to spatial drift of the sample stage during analysis, measurements were divided into numerous planes and shifts between individual image planes were corrected. We used a primary Cs^+ ion beam with 16 keV (6f: 17.5 keV) and currents of typically 0.5 to 2 pA (6f: 10 to 40 pA). Prior to data collection, all samples were exposed for several minutes to a higher Cs^+ current of 100 to 400 pA to remove surface contamination, increase the work function and reach sputtering equilibrium. Primary beam diameters, and hence approximate spatial resolutions, were typically 100 nm for the NanoSIMS and 1 μm for the ims-6f measurements. Hydrogen isotopes were measured along with ^{12}C and $^{16/18}O$ with the ims-6f in peak-jumping mode: count rates were interpolated between image planes to take into account temporal drift. Carbon and N isotopes were measured in Mainz with simultaneous detection of negative ions of ^{12}C, ^{13}C, $^{12}C^{14}N$, $^{12}C^{15}N$ and ^{30}Si. Presolar grains were searched for in all IDPs except for P2

Table 1
H and N isotope anomalies and C Raman band parameters in the IDPs.

Sample			δD (‰)		$\delta^{15}N$ (‰)		D band (cm^{-1})		G band (cm^{-1})	
Collector			Bulk	Hotspot max.	Bulk	Hotspot max.	Width	Position	Width	Position
L2054	Cluster 1	E1#1	4310 ± 460	12,700 ± 1900	395 ± 10	1290 ± 140	368.7 ± 1.2	1362.0 ± 0.3	127.5 ± 0.3	1569.7 ± 0.3
		E1#2	8700 ± 1000	21,500 ± 3600	485 ± 35	1310 ± 150	396.1 ± 5.7	1361.1 ± 1.1	136.8 ± 1.3	1565.8 ± 0.7
				29,300 ± 5800[a]						
		E1#3	2860 ± 480	9500 ± 3200			367.3 ± 3.0	1363.8 ± 0.8	129.2 ± 0.9	1569.2 ± 0.5
		E1	4430 ± 480	29,300 ± 5800	405 ± 10	1310 ± 150				
L2054	Cluster 1	F1	2600 ± 140	4100 ± 400	n.d.	n.d.	344.0 ± 1.2	1363.8 ± 0.3	128.3 ± 0.3	1563.3 ± 0.2
L2054	Individual	G2	1370 ± 200	9900 ± 1200	395 ± 10	1470 ± 220	291.4 ± 1.0	1357.4 ± 0.3	115.4 ± 0.4	1580.2 ± 0.3
				29,300 ± 12,700[b]						
L2054	Individual	G3	190 ± 110	4400 ± 850	25 ± 20	950 ± 390	287.6 ± 1.0	1353.7 ± 0.4	115.0 ± 0.7	1585.5 ± 0.3
L2054	Individual	G4	2500 ± 340	12,900 ± 1800	145 ± 15	410 ± 80	362.1 ± 9.6	1358.7 ± 1.3	131.3 ± 2.1	1569.9 ± 1.2
L2054	Cluster 2	P2	n.d.				319.2 ± 8.1	1346.9 ± 3.4	148.3 ± 3.8	1562.3 ± 1.4
L2036	Cluster 9	P1A	420 ± 170	1300 ± 450	70 ± 20		n.d.	n.d.	n.d.	n.d.
		P1B	570 ± 200	2100 ± 600	250 ± 30	940 ± 140	n.d.	n.d.	n.d.	n.d.
L2036	Cluster 20	20P3	860 ± 220	1120 ± 300	460 ± 20	1400 ± 300	295.6 ± 5.7	1346.3 ± 1.3	146.9 ± 2.6	1575.3 ± 0.7
L2036	Cluster 20	20P4	1540 ± 290	3100 ± 500	401 ± 6	930 ± 120	259.5 ± 20.4	1343.8 ± 4.6	163.1 ± 15.0	1576.2 ± 2.2
L2036	Cluster 3	3P1	n.d.				318.6 ± 18.4	1364.3 ± 4.4	128.9 ± 6.4	1566.0 ± 2.7
L2036	Cluster 3	3P2	n.d.				344.5 ± 4.7	1357.5 ± 1.6	136.5 ± 2.5	1563.3 ± 0.9
L2036	Cluster 3	3P3	n.d.				271.0 ± 15.2	1335.7 ± 3.4	180.7 ± 8.1	1559.5 ± 1.8
L2036	Cluster 3	3Px	n.d.				297.3 ± 4.2	1347.6 ± 1.9	118.4 ± 2.3	1572.3 ± 1.0
L2036	Cluster 9	9P3	n.d.				276.5 ± 3.6	1345.9 ± 0.9	113.8 ± 2.6	1579.2 ± 1.2
L2036	Cluster 9	9P4	n.d.				252.6 ± 2.0	1349.9 ± 0.6	106.2 ± 1.0	1584.5 ± 0.4
L2036	Cluster 9	9P5	n.d.				251.7 ± 4.0	1357.2 ± 0.9	121.0 ± 2.5	1586.3 ± 1.1
L2036	Cluster 9	9P6	n.d.				229.8 ± 3.6	1345.5 ± 1.7	121.6 ± 6.3	1587.2 ± 1.3

[a] Sub-region of D-rich hotspot in section E1-A.
[b] A repeat measurement with more planes revealed a smaller enrichment ($\delta D/H = 9900 \pm 2600$‰) indicating that this D-rich OM was superficial and partially sputtered away during SIMS analysis.

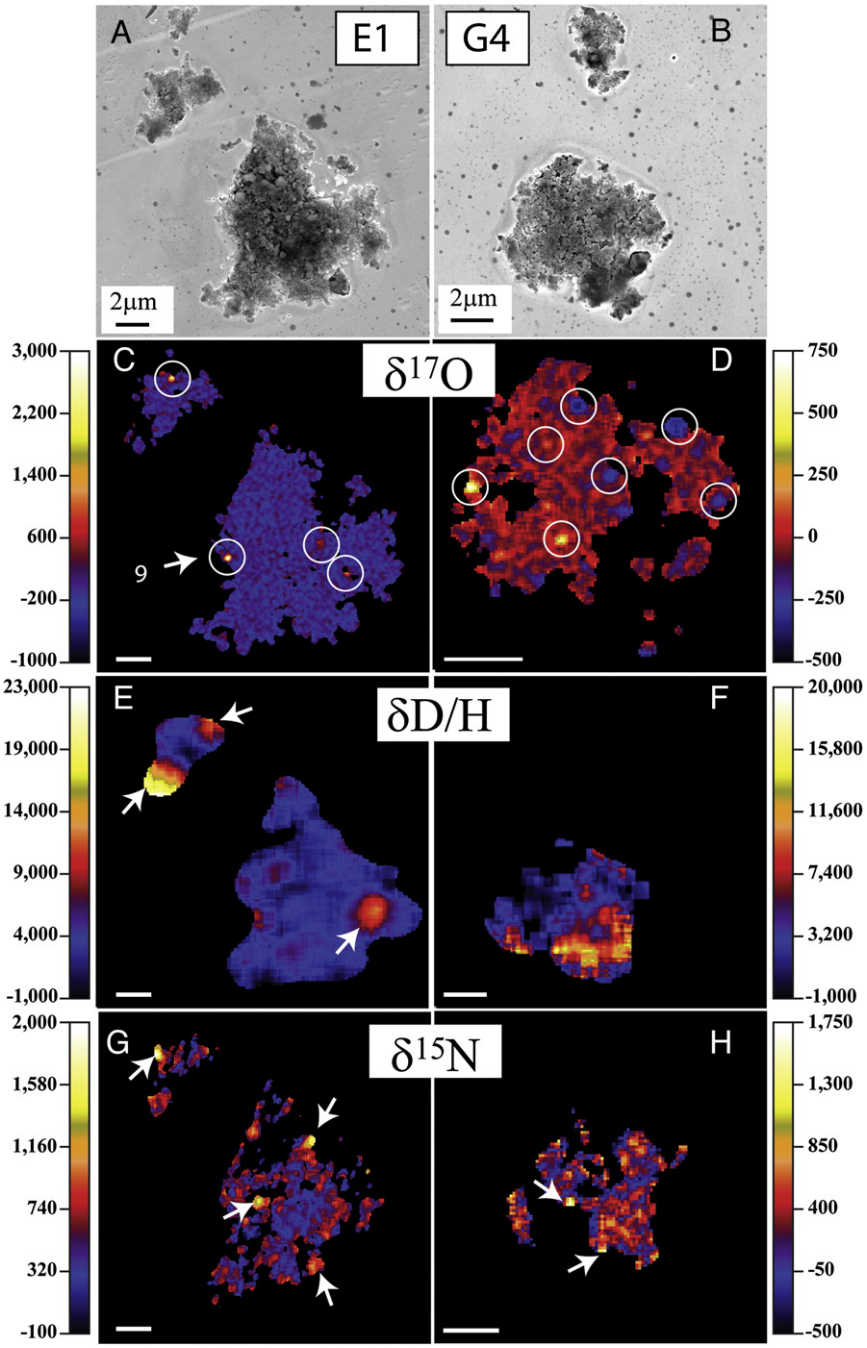

Fig. 1. Scanning electron images of Grigg–Skjellerup Collection IDPs E1 (panel A) and G4 (B) and secondary ion mass spectrometry (SIMS) isotopic ratio maps (C–G). The IDPs are particularly fine-grained—typical for unprocessed chondritic porous IDPs—and consist of various mainly anhydrous minerals, glassy silicates and organic coatings that may act as "glue" between the phases. $\delta^{17}O/^{16}O$ maps of IDPs E1 (C) and G4 (D) show four and seven isotopically anomalous regions, respectively (Fig. 3). These grains are identified as presolar silicates because the O isotopic anomalies are spatially correlated with Si. Presolar grain #9 (C) is olivine (Fig. 4). SIMS maps of the H (E, F) and N (G, H) isotopic compositions show localised so-called "hotspots" (arrows) with δD and $\delta^{15}N$ values up to 21,000‰ and 1300‰, respectively (Table 1). The H isotopic ratio images were acquired using the ims-6f and thus have lower spatial resolution. Variations in isotopic ratios are given as deviations from terrestrial standards in permil ($\equiv\delta$ notation). The scale bars are 2µm.

(Table 1) by simultaneous mapping of ^{12}C, $^{16/17/18}O$, $^{12}C^{14}N$, ^{28}Si negative ions and secondary electrons. Two IDPs with identified presolar grains were subsequently re-analyzed for their Si isotopic compositions; $^{28,29,30}Si$ and $^{24}Mg^{16}O$ were measured along with ^{16}O and ^{17}O to precisely locate the presolar grains. All data were corrected for electron multiplier deadtime. For the H, C and N measurements, instrumental mass fractionation (IMF) was corrected for with well-characterized terrestrial samples and meteoritic insoluble organic matter (IOM) (Alexander et al., 2007a). O- and Si-isotopic data were internally normalized to the average composition of non-presolar material within each image. Moreover, the effect of quasi-simultaneous arrival (Slodzian et al., 2004) on the O-isotopic data was empirically corrected by fitting the linear relationship between pixel isotope ratios and ^{16}O count rates. Quoted uncertainties are based both on counting statistics and the uncertainty in the IMF.

2.4. Raman spectroscopy

Raman spectroscopy is relatively non-destructive and requires little sample preparation, which renders this method very useful for the analyses of fragile IDPs. IDPs have previously been examined at a bulk particle scale (~5 to 10 µm) (Wopenka, 1988; Quirico et al.,

2005). Our study uses the WiTec alpha-SNOM micro-Raman spectroscope at the Carnegie Institution (Busemann et al., 2007). This instrument uses a Nd:YAG laser with 532 nm wavelength in a backscattering geometry and a confocal setup that provides a significant reduction of fluorescence. To avoid thermal modification of the samples, laser power was limited to ~55 μW. Data were acquired in imaging mode with sub-micron spatial resolution, which allows spectra to be obtained from the most C-rich regions within the IDPs. Some IDPs discussed in this work have been analyzed with SIMS prior to the Raman spectroscopic examinations. This is not ideal because high-energy Cs^+ ion implantation during SIMS inevitably induces amorphization within the top layers of the irradiated material. However, we can exclude that this amorphization mimicked a more primitive character of the analyzed organic matter (OM) because (i) additional IDPs from the Grigg–Skjellerup collectors that were analyzed with the same Raman instrumental settings but were not examined with SIMS show similarly primitive OM (Busemann et al., 2009); (ii) all IDPs analyzed in this work experienced roughly the same dose of Cs^+ ion implantation and, hence, comparable amorphization; (iii) Raman characteristics of meteoritic IOM with and without Cs^+ ion implantation during SIMS analysis show that laboratory-induced shifts towards a more primitive character are significantly smaller than the differences observed in the IDPs discussed in this work; and (iv) the observed correlation between bulk D/H ratios and Raman band parameters for the GSC-IDPs suggests that the differences in Raman spectra are intrinsic to the samples. Data were fitted with Lorentzian profiles for the Raman bands with a free-floating linear background using custom software written in the IDL programming language (Research Systems Inc.). Spectra showing strong fluorescence were excluded (Busemann et al., 2007).

2.5. Focused ion beam scanning electron microscopy (FIB-SEM)

We used an FEI Nova 600 focused-ion-beam scanning-electron microscope (FIB-SEM) at the Naval Research Laboratory (NRL) to prepare electron-transparent cross sections of the IDP fragments (Fig. S2) for transmission electron microscope (TEM) and X-ray analysis. Protective straps of Pt were deposited on top of the IDP fragments within the FIB to mitigate radiation damage and Ga^+ implantation during ion milling and oriented so that they transected the isotopic hotspots that were identified by SIMS (Fig. 2). Six FIB sections were extracted from IDPs E1 and G4 and thinned to electron transparency (≤150 nm) in situ using established methods (Zega et al., 2007), though only three were successfully analyzed by TEM and STXM. All examined particles showed mild to severe sputtering loss from SIMS analysis. This prevented the analysis of some of the presolar grains (Table 2), e.g., presolar silicates in sections E1-A and G4-C and the "X-grain" #12 in G4-A (Fig. 2B, blue arrow).

2.6. Transmission electron microscopy (TEM)

All FIB sections were examined with a 200 keV JEOL2200FS transmission electron microscope (TEM) at NRL, equipped with an ultra-thin-window Noran energy-dispersive X-ray spectrometer (EDS), bright- and high-angle annular dark-field (HAADF) scanning TEM (STEM) detectors, and an in-column electron energy-loss spectrometer. Grain chemistry was measured using the EDS detector and processed with Noran System Six software. Depending upon illumination conditions, the spectral acquisition time was varied between 1 and 5 min to ensure good counting statistics (high count rate with deadtime ≤30%). Selected-area electron-diffraction (SAED) patterns were acquired, where possible, from individual grains. All SAED patterns were measured, both digitally and manually, with Adobe Photoshop and the crystallographic image processing software package CRISP (Hovmöller, 1992), based on calibrated camera constants. The indexing of the SAED patterns was based on comparison

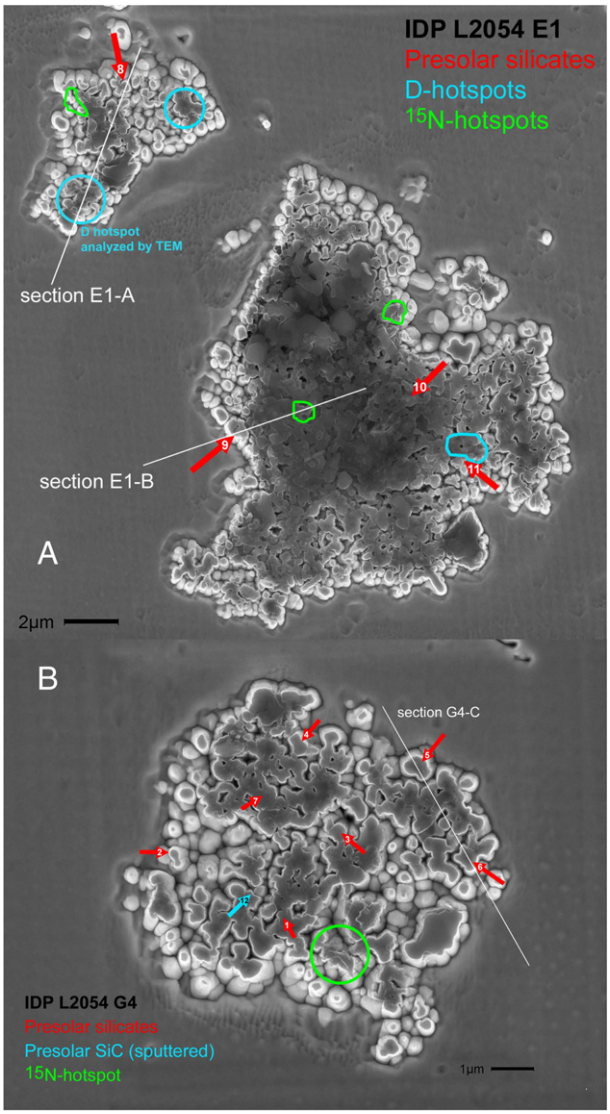

Fig. 2. Secondary electron images of IDPs E1 (A) and G4 (B), isotopically anomalous areas (outlines and arrows) and location of FIB-SEM lift-out sections (white lines). The extremely D-rich region (,000‰) in section E1-A contains a fine-grained heterogeneous mixture of amorphous and crystalline phases (Fig. 8). Section E1-B transects a presolar Mg-rich olivine grain (#9, Fig. 4) and a ^{15}N hotspot associated with very fine-grained material. Section G4-C (panel B) transects two presolar silicate grains. This IDP also contains a grain that is most likely a presolar SiC (grain #12) that has been sputtered away by SIMS, and a ^{15}N-rich organic hotspot.

with known structure types and, where necessary, patterns calculated using JEMS multislice simulation software (Stadelmann, 1987). Phase identification was based, where possible, on both measurements from X-ray spectra and SAED patterns. However, the small sizes (<50 nm) of some grains precluded acquisition using a selected-area aperture, and in such cases, phase identification was based on STEM-based X-ray spectrum images.

2.7. X-ray absorption near-edge structure spectroscopy (XANES)

Synchrotron-based XANES analyses of the X-ray transparent sections E1-A and E1-B were performed on the scanning transmission X-ray microscope (STXM) (Kilcoyne et al., 2003) located at beamline 5.3.2 of the Advanced Light Source (ALS, Lawrence Berkeley National Laboratory). Beamline 5.3.2 employs a bending magnet spanning the energy range of 270 to 800 eV that enabled us to obtain X-ray

Table 2
Identified presolar grains in GSC-IDPs E1 and G4.

IDP	Grain #	FIB section	$^{17}O/^{16}O \times 10{,}000$	$^{18}O/^{16}O \times 10{,}000$	$\delta^{29}Si$ (‰)	$\delta^{30}Si$ (‰)	Appr. size/(μm [a])	Mineralogy [b]	Isotope group
G4	1	A[c]	5.72 ± 0.18	16.6 ± 0.6	−47 ± 23	3 ± 29	0.32	Silicate	1
	2	A	6.54 ± 0.23	19.9 ± 1.1	77 ± 34	52 ± 42	0.28	Silicate	1
	3	B[c]	2.87 ± 0.14	18.5 ± 0.6	−8 ± 21	−72 ± 25	0.28	Silicate	3
	4	B	2.62 ± 0.13	19.3 ± 0.5	67 ± 26	95 ± 28	0.31	Silicate	3
	5	C	2.74 ± 0.08	18.3 ± 0.5	27 ± 17	26 ± 21	0.45	Silicate	3
	6	C	3.06 ± 0.12	17.6 ± 0.6	−54 ± 25	−18 ± 32	0.30	GEMS?	3
	7	[d]	4.63 ± 0.20	19.7 ± 0.7	38 ± 32	52 ± 39	0.21	Silicate	1
E1	8	A	15.75 ± 0.29	19.0 ± 1.2	149 ± 25	133 ± 30	0.36	Silicate	1
	9	B	11.81 ± 0.22	21.1 ± 0.7	28 ± 20	12 ± 25	0.35	Olivine	1
	10	B	7.22 ± 0.10	14.7 ± 0.4	4 ± 10	5 ± 12	0.50	Silicate	1
	11	C	7.42 ± 0.17	22.5 ± 1.2	24 ± 17	70 ± 21	0.34	Silicate	1
G4	12	A	–	–	−159 ± 25	−74 ± 39	0.24	SiC?	X grain

[a] Determined with the NanoSIMS O isotope maps.
[b] In contrast to the olivine and possible GEMS identifications, the grain "mineralogy" was elsewhere estimated by the $^{28}Si/^{16}O$ ratio from the NanoSIMS. According to the $MgO/^{16}O$ NanoSIMS ratio, all grains appear to have some Mg.
[c] Not yet extracted.
[d] Not contained in a FIB section.

absorption spectra at the C, N, O and Fe K-edges and the Ca L-edge. Fresnel zone-plate optics provide focusing of the monochromatic beam to a spot size of 30 nm. Our analyses were performed using the "stack technique", where spectral image sets are acquired for 50 to 100 nm^2 pixels spanning an area of several square microns with the energy range spanning the absorption edge of interest, e.g., 270 to 340 eV for C. Absorption (A) is the ratio of the X-ray transmission (I) at a given energy to the incoming X-ray intensity (I_0): $A = -\log(I/I_0)$. The transmitted photons are collected with a photomultiplier. The X-ray energy (resolving power $E/\Delta E$ ~5000) is tuned in ~100 to 300 steps (step size between 0.1 and 1 eV) over the respective edge energies of C, Ca, N, O and Fe at 290, 350, 405, 540 and 720 eV, respectively. Spectral assignments for various peaks in the pre-edge region of the carbon K edge to functional groups are summarized by Cody et al. (2008). The spectral data cubes were reduced with the IDL software package aXis2000 (A. P. Hitchcock, McMaster University, Hamilton ON, Canada, http://unicorn.mcmaster.ca/aXis2000.html), which allows shift correction during stack acquisition, normalization to the incoming X-ray intensity, and the selection of regions-of-interest.

3. Results

3.1. General observations

Scanning electron microscopy (SEM) indicates that the IDPs found on the Grigg–Skjellerup dust stream collectors (GSC-IDPs) are fine-grained, low-density, "chondritic porous" IDPs (Fig. 1A–B and S1A–B). Such samples are typically dominated by anhydrous minerals and abundant carbonaceous material (Bradley, 2003). We analyzed both "cluster" and "individual" IDPs (Table 1). Cluster IDPs are large (50 to 500 μm) fragile aggregates that disintegrate into many fragments during collection, whereas individual IDPs occur as isolated grains on the collectors (Bradley, 2003). It was argued that cluster IDPs are generally more primitive than individual IDPs based on a wider range of H and N isotopic anomalies in the former (Messenger, 2000; Messenger et al., 2003b).

3.2. Presolar grains

SIMS $\delta^{17}O/^{16}O$ maps for cluster fragment E1 and individual IDP G4 are shown in Fig. 1C–D. Four sub-micron-sized regions in E1 and seven in G4 show extreme O isotopic anomalies (Table 2) indicating that they are presolar grains that condensed around previous generations of stars. SIMS analysis did not reveal any isotopically anomalous region in O or Si in the other IDPs analyzed. SIMS, SEM and, in some cases, TEM analyses of the presolar grains from E1 and G4 show that they are all silicates. The O and Si isotopic compositions of these 11 presolar grains are within the ranges observed previously for presolar grains in meteorites and other IDPs (Nittler et al., 1997; Nittler, 2003; Messenger et al., 2003a; Nguyen et al., 2007; Vollmer et al., 2008) (Fig. 3).

The seven ^{17}O-rich ("Group 1") grains likely formed in winds of low-mass asymptotic giant branch stars (Nittler, 2003), whereas the origin of the four ^{17}O-depleted ("Group 3", Nittler, 1997) grains is more ambiguous. Most Group 3 presolar oxide grains are believed to have formed in low-metallicity low-mass red giants (Nittler et al., 1997). However, the Group 3 silicate grains from G4 belong to a sub-group with $^{17}O/^{18}O$ ratios lower than the solar value and such grains cannot be easily explained as having originated in low-mass stars. Rather, Nittler et al. (2008) recently argued that these unusual grains are related to the ^{18}O-rich Group 4 grains and likely formed in one or more supernovae.

The Si isotopic compositions of most of the analyzed presolar grains fall on the same correlation line defined by mainstream presolar SiC grains (Fig. 3B) and are believed to largely represent the Galactic chemical evolution of the Si isotopes through time (Alexander, 1993). The Si-isotopic compositions of the Group 3 grains from G4 are not particularly diagnostic of their origins, both because a wide range of Si-isotopic compositions might be expected for supernova grains, depending on the precise mixture of the SN zones (Hoppe et al., 2009, and references therein), and because the data are somewhat compromised by contributions from surrounding, isotopically normal material. NanoSIMS imaging of G4 also revealed a sub-micron region highly enriched in ^{28}Si, but with normal O isotopic ratios (Grain #12, Table 2). We tentatively identify this as a presolar SiC grain of type X (Nittler, 2003) (Fig. 3B). However, it was severely sputtered during the SIMS analysis (Fig. 2B) and could not subsequently be identified in the section.

One of the presolar grains (#9) in section E1-B (Fig. 4A) was identified by TEM analysis as crystalline Mg-rich olivine (Fig. 4B–C). This grain is in contact with amorphous C-rich material including a ~50 nm-sized structure that resembles a carbonaceous nano-globule (Garvie et al., 2008). Nano-globules are abundant carriers of large D and ^{15}N enrichments in primitive meteorites, and, hence, are likely of interstellar origin (Nakamura-Messenger et al., 2006). Similar to the anomalous OM discussed below, XANES results imply that Ca-bearing carbonates are also embedded in the OM adjacent to the presolar olivine, as well as in ^{15}N-enriched OM that is in close proximity to this region (Fig. 4A). A presolar supernova olivine partially embedded in ^{15}N-rich organic coating has been observed previously in another IDP (Messenger et al., 2005).

Unfortunately, insufficient material remained of the presolar silicate #8 in section E1-A (Fig. 2A) for TEM analysis. EDS on presolar silicate #6 from section G4-C (Fig. 2B) suggests that silicate material is present. However, it was impossible to distinguish any crystalline signal in the bright-field TEM image. This grain might be a GEMS (glass with embedded metal and sulfides) particle, a major component of IDPs (Bradley, 2003), but the data are inconclusive and the unfortunate loss of this section prevents any further examination.

The nominal abundance of presolar silicates is extremely high in the GSC-IDPs, particularly in E1 (0.35%) and G4 (1.5 wt.%), the largest observed in any extraterrestrial material (Fig. 3C). Clustering of presolar grains has been seen in other extraterrestrial materials (Yada et al., 2008; Floss and Stadermann, 2009), but the density of grains in E1 and G4 is vastly higher. Using a binomial distribution, we conservatively estimate the probability of finding 11~300 nm presolar grains in IDPs E1 and G4 (area ~250 μm^2) to be well below 10^{-8}, if the true abundance of presolar grains were only 375 ppm, as previously inferred for the most isotopically primitive IDP subset (Floss et al., 2006). This result proves the extremely primitive character of these IDPs, and, together with their isotopically anomalous organic material (see below), demonstrates that sizeable aggregates of interstellar origin can survive in IDPs. Even including the less primitive G2 and G3, the abundance of presolar silicate grains in all analyzed IDPs from collector L2054 is found to be ~500 ppm (Fig. 3C), still higher than the estimates for other primitive materials, e.g., 375 ppm in isotopically primitive IDPs, ~120 ppm in all IDPs (Floss et al., 2006), and 100 to 200 ppm in the most presolar grain-rich meteorites, the carbonaceous chondrites Acfer 094, Meteorite Hills 00426 and Queen Elizabeth Range 99177 (Nguyen et al., 2007; Vollmer et al., 2008; Floss and Stadermann, 2009). In comparison, only three presolar silicate grains have been found in Wild 2 dust analyzed to date, giving a rough estimate of 17 ppm (McKeegan et al., 2006; Stadermann and Floss, 2008), possibly due to alteration during capture (Stadermann et al., 2009).

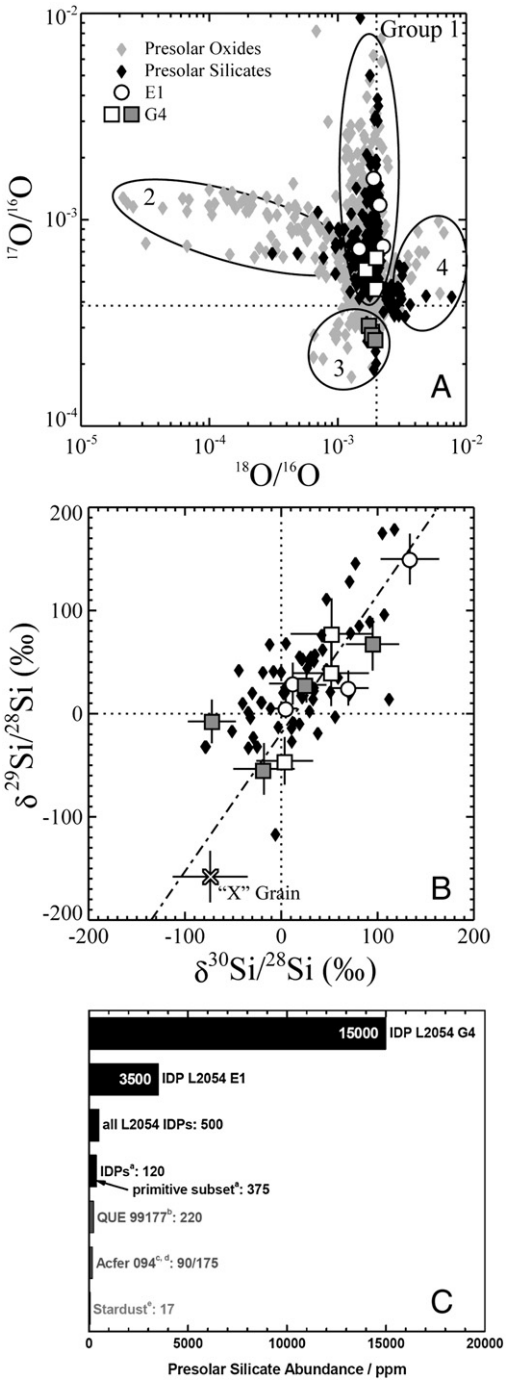

Fig. 3. Oxygen (A) and Si (B) isotopic compositions of the presolar grains in IDPs E1 and G4 compared to those previously measured in presolar oxide and silicate grains in other samples (Nittler et al., 1997; Nittler, 2003; Messenger et al., 2003a; Mostefaoui and Hoppe, 2004; Nguyen et al., 2007; Vollmer et al., 2008). All four presolar grains in IDP E1 and three from G4 have O isotopic compositions placing them in the most common group (Group 1) of presolar oxides and silicates (Nittler, 2003). In contrast, four grains in G4 belong to the rare ^{16}O-enriched Group 3. Such clusters may imply that these IDPs inherited assemblages of presolar and primitive materials that were less homogenized in the early solar system than those found in the asteroidal parent bodies of meteorites. The Si isotopic compositions (B) of all 12 presolar grains plot close to the correlation line (dashed) observed in mainstream presolar SiC grains (Nittler, 2003), reflecting galactic chemical evolution of the Si isotopes. The presolar grain labelled "X" has a Si isotopic composition similar to that of SiC X grains, believed to have condensed in supernova outflows. (C) IDP G4 contains presolar silicates at an extreme nominal percent level, the largest abundance observed in any extraterrestrial material, illustrating the pristine character. All GSC-IDPs analyzed here with SIMS yield an average presolar silicate abundance of ~500 ppm, larger than abundances found as yet in any extraterrestrial material, such as average (non-GSC) IDPs, a primitive, ^{15}N-rich subset of these IDPs, and the matrices of very presolar silicate-rich meteorites Acfer 094, MET 00426 and QUE 99177. As yet analyzed comet Wild 2 dust contains comparatively few presolar grains. References: [a] Floss et al. (2006), [b] Floss and Stadermann (2008), [c] Nguyen et al. (2007), [d] Vollmer et al. (2008), [e] Stadermann and Floss (2008).

3.3. Isotopically anomalous organic matter

Organic matter (OM) in the GSC-IDPs exhibits significant enrichments in D and ^{15}N relative to H and ^{14}N and terrestrial isotopic ratios. IDPs are generally rich in D and ^{15}N (Messenger, 2000; Messenger et al., 2003b), testifying to their primitive characteristics (Floss et al., 2006). However, the magnitudes of the ^{15}N and especially the D anomalies observed here in the GSC-IDPs are unusually high even for primitive IDPs (Table 1) and are comparable to OM extracted from the most primitive meteorites (Busemann et al., 2006a). Fig. 5 compares the range of D/H ratios observed in the GSC-IDPs to those of other IDPs analyzed by the same scanning ion imaging technique used here.

The bulk $\delta D/H$ value for IDP E1 (~4400‰, Fig. 5) exceeds the maximum bulk value observed in all but two of 20 other cluster IDPs analyzed by the same technique. Only one IDP (Messenger, 2000) has been previously reported with a D hotspot as enriched as the maximum value observed in E1 (Fig. 1E, hotspot ~21,000‰). The individual GSC-IDPs are also atypically D-rich; hotspot D/H values in G4 and G2 are higher than have been reported in any other individual IDP: a small hotspot in G2 reaches 32,000‰. The bulk D/H ratios of G2 and G4 are also higher than those of other IDPs (Table 1, Fig. 5).

The ranges of ^{15}N/^{14}N ratios detected in the GSC-IDPs largely overlap with those seen in previous IDP studies (Messenger, 2000; Messenger et al., 2003b; Aléon et al., 2003; Floss et al., 2004, 2006). Bulk δ^{15}N values for the analyzed GSC-IDPs are at the high end of all

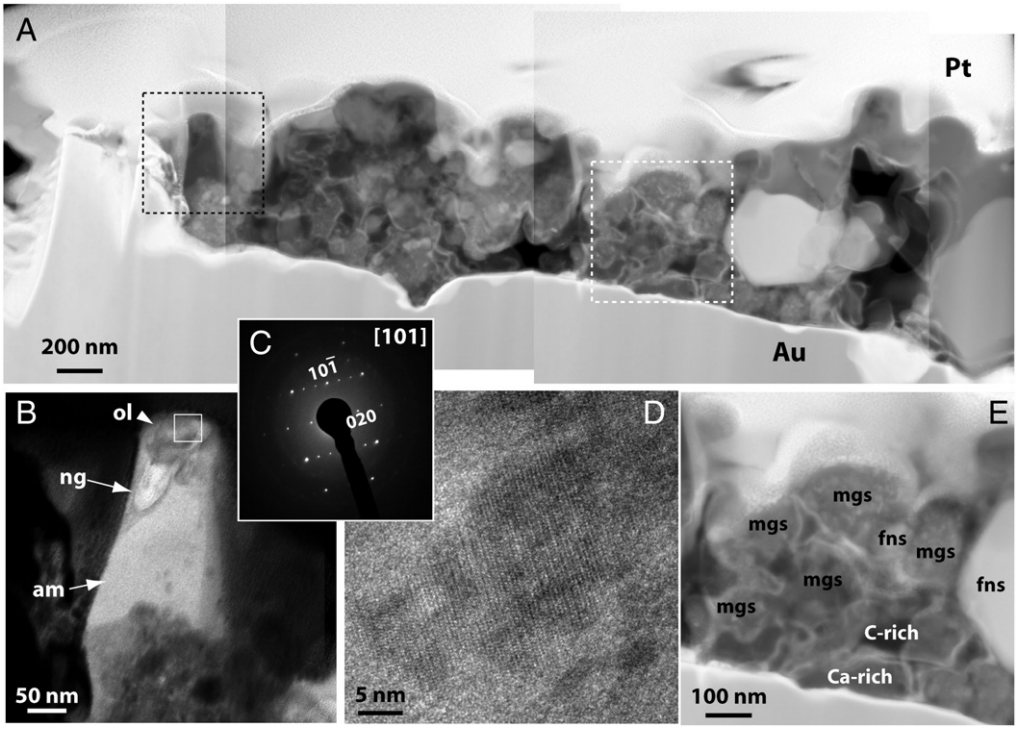

Fig. 4. TEM data on the FIB section E1-B. (A) HAADF image showing the overall IDP sandwiched between Pt strap and Au foil. The black and white boxes indicate the locations of presolar grain #9 enriched in ^{17}O, indicating an origin in a low-mass red giant star (Nittler et al., 1997), and a ^{15}N-rich hotspot, respectively. (B) Bright-field TEM image of the area enclosed by the dashed-black box in (A). Olivine (ol) occurs with amorphous probably carbonaceous material (am) and a particle with a nano-globule-like (ng) morphology. (C) SAED pattern acquired from the olivine grain (white box in panel B) and indexed to monticellite, a Ca-bearing olivine. (D) HRTEM image of the olivine grain and surrounding glass. (E) HAADF image of the area enclosed by the dashed-white box in (A). Spectrum imaging reveals that magnesium silicates (mgs), Fe–Ni sulfide (fns), and C- and Ca-rich material occur in the ^{15}N-rich hotspot.

reported values. Only one IDP reported by Floss et al. (2006) shows a higher bulk value than E1 and G2. Moreover, hotspot values in E1 and G2 (δ^{15}N > 1300‰) are higher than any previously observed in IDPs.

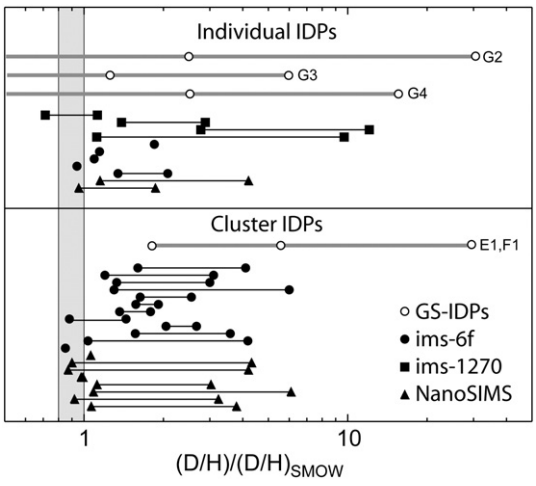

Fig. 5. Ranges of D/H ratios in IDPs. D/H ratios measured in the GSC-IDPs are higher than typical values for IDPs measured previously using the same analytical technique (scanning ion imaging) with three different ion microprobes. Each line indicates the range of *D/H* ratios in a single IDP. For GSC-IDPs, open circles indicate bulk, minimum and maximum hotspot values. For Cameca ims-6f (Nittler and Messenger, 1998; Mukhopadhyay et al., 2002; Mukhopadhyay and Nittler, 2003; this work; unpublished data from CIW), and Cameca ims-1270 (Aléon et al., 2001) measurements, plotted values represent ranges of micrometer-sized sub-regions of the samples. For literature NanoSIMS measurements (Floss et al., 2006), lower values represent bulk compositions, while higher values represent maximum hotspot values. The earlier observed trend that cluster IDPs contain more pristine D-rich organic matter than individual IDPs (Messenger et al., 2003b) appears less distinct. The shaded area defines D/H in terrestrial samples.

In addition to H and N we analyzed the C isotopic composition of the GCS-IDPs. While presolar graphite or SiC grains often show large isotope anomalies with ^{13}C/^{12}C ratios that are typically more than 50% smaller or larger than the terrestrial composition (Nittler, 2003), δ^{13}C ratios of C isotopic anomalies in OM are typically in the range of ± 100‰ (Floss et al., 2004, 2006; Nakamura-Messenger et al., 2006; Busemann et al., 2006a) and, hence, more difficult to detect. Some of these relatively rare anomalies have been associated with nano-globules and monolithic amorphous C (Busemann et al., 2006b; Nakamura-Messenger et al., 2006). Distinction from isotopically anomalous presolar graphite is impossible without structural analysis.

All GSC-IDPs analyzed here with NanoSIMS show C isotopic anomalies, demonstrating the IDPs' non-homogenized, pristine character. The extremely D-rich hotspot in IDP E1 (see also next section) contains, e.g., three small regions with δ^{13}C ~ −280‰ and is also slightly enriched in ^{15}N (~600‰), relative to its bulk value (δ^{15}N ~400‰). The bulk δ^{13}C values between −9 and −51‰ are in the typical range observed previously in IDPs (Messenger et al., 2003b; Floss et al., 2006).

The data do not show any obvious correlations between isotopic and elemental compositions (i.e. C/H ratio or N abundance, Fig. S3), which would be expected if the IDPs analyzed here contain OM similar to the components OM1–OM3 suggested previously for IDPs (Aléon et al., 2003). Rather, the lack of correlations implies a diversity of organic materials that are intermixed on very fine scales in the analyzed samples.

Raman spectroscopy was used previously to investigate the relative degree of disorder or maturity of OM in IDPs (Wopenka, 1988). The peak parameters (relative size, widths, and positions) of the so-called D and G bands (Fig. 6) are correlated with alteration processes that the OM experienced. These processes could include amorphization, e.g., due to irradiation in space, thermal metamorphism experienced on parent bodies and changes in the chemical composition (Busemann

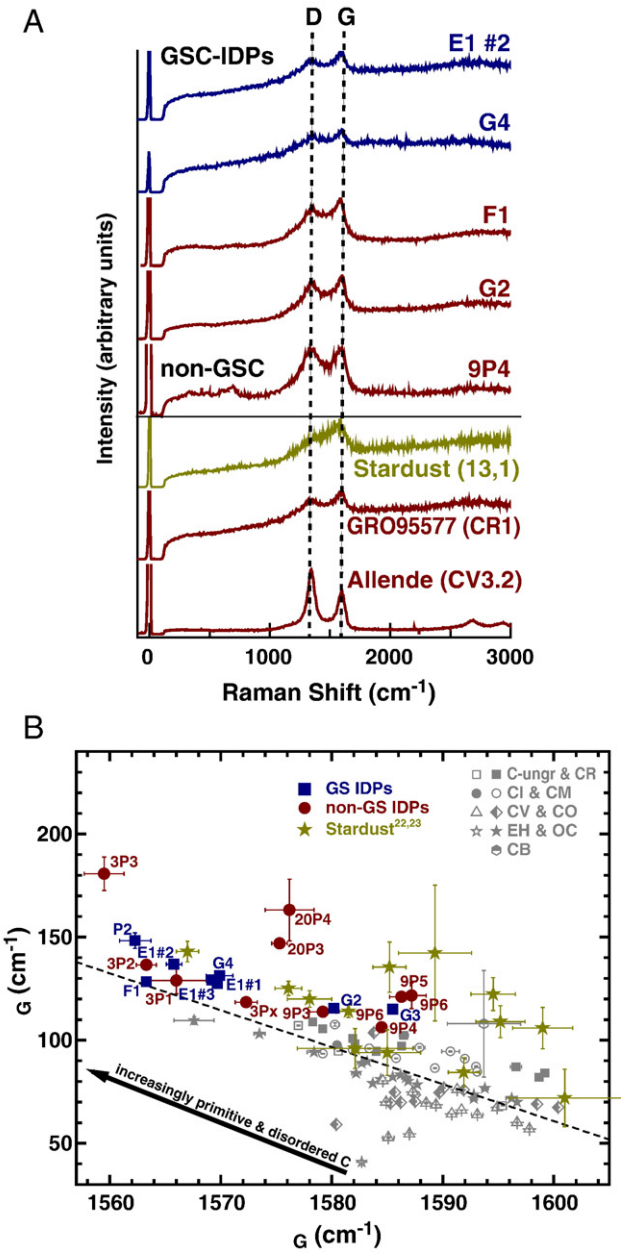

Fig. 6. Raman spectroscopic results from GSC-IDPs, meteorites, and Wild 2 (Stardust) samples. (A) Organic matter (OM) in IDPs G4 and E1 is very disordered, showing very primitive (=broad) Raman carbon D and G bands (Table 1). The IDP spectra are compared with those from primitive (GRO 95577) and altered (Allende) chondritic OM (Busemann et al., 2007) and Wild 2 OM (Sandford et al., 2006; Rotundi et al., 2008). (B) Meteoritic OM produces a linear trend (dashed line) in the G band Raman parameter plot (band widths Γ vs. positions ω) that follows parent body thermal metamorphism (Busemann et al., 2007). More metamorphosed samples plot to the lower right, while meteorites that contain more primitive OM (e.g., CI, CM, and CR chondrites) plot towards the upper left. Data points of many GSC- and other IDPs plot further up the linear trend than the most primitive meteorites, implying extremely primitive OM in these IDPs.

et al., 2007). Generally, as the degree of disorder of the OM increases, the D and G band widths get broader and the G band position moves towards lower wavenumbers. Pure graphite shows solely a narrow G band around 1582 cm^{-1}. Detailed studies on IOM in primitive meteorites show that the C Raman parameters can be used to assess and compare the metamorphic degree of meteorites within the same chemical class (Busemann et al., 2007).

Fig. 6A shows that the OM in the GSC-IDPs is disordered and primitive, comparable to previous studies on IDPs (Quirico et al., 2005), Wild 2 dust (Sandford et al., 2006; Rotundi et al., 2008), and meteoritic insoluble OM (Busemann et al., 2007). In particular, the related cluster IDPs E1 (3 fragments) and F1, and individual IDP G4 lie in the upper left of the Raman G band parameter plot (Fig. 6B), reflecting the presence of highly disordered C. We can exclude that these primitive characteristics are due to amorphization of the C during the SIMS analyses (Section 2.4). The slightly less primitive Raman spectra of G2 and G3 are comparable to those observed in many meteorite classes and are consistent with their less anomalous bulk H isotopic compositions compared to E1 and G4.

C-XANES reveals that the OM in E1 associated with D and ^{15}N enrichments is not highly aromatic relative to macromolecular OM found in meteorites (Cody and Alexander, 2005) and is relatively rich in O-bearing functional groups, evident by the intense vinyl-ketone and carboxyl peaks (Fig. 7A). Both observations combined suggest that this OM is particularly pristine (Sandford et al., 2006; Cody et al., 2008), in agreement with its high δD and $\delta^{15}N$ values and extremely disordered Raman signature.

3.4. Extreme D-rich hotspot in IDP E1

Large D enrichments relative to terrestrial H isotopic composition have been found in many primitive IDPs, which most likely indicate the preservation of non-homogenized presolar materials (Messenger et al., 2003b). Generally, D hotspots are associated with poorly ordered aliphatic carbon (Keller et al., 2004). Often, extremely fine-grained minerals including silicates, sulfides and GEMS are embedded in the D-rich organic matter. It is highly debated whether GEMS are (Bradley et al., 1999; Keller et al., 2000) or are not (Keller and Messenger, 2004, 2008) of presolar origin too.

Fig. 8A shows a Z-contrast scanning transmission electron image of section E1-A, containing one of the most D-enriched regions in all IDPs (δD ~21,000‰, $\delta^{13}C$ ~−130‰, $\delta^{15}N$ ~600‰). Bright-field and HAADF images show that the D-rich region contains a heterogeneous mixture of material (Fig. 8B). The material in this area consists of low-Mg/Si glass, typical for GEMS, crystalline silicates (Ca-bearing polycrystalline pyroxene and Mg silicates), and Fe–Ni metal and sulfides. This fine-grained assemblage measures ~700 nm × 700 nm and shows features that are commonly found in GEMS (Bradley, 2003). The SAED pattern (Fig. 8E) from a large grain (Fig. 8C, white dashed circle) reveals two sets of reflections showing that the grain is polycrystalline. The SAED pattern is consistent with monoclinic pyroxene. HAADF and EDS data show that the grain is uniformly composed and contains Mg, Ca, Fe, Na, Si and O.

Interestingly, the D-rich GEMS-like region also contains a small (~90 nm) grain (Fig. 8C, black dashed circle, Fig. 8H) whose SAED pattern (Fig. 6G) indexes to anthophyllite amphibole: EDS shows that this grain contains Fe, Mg, Si and O. Measurement of its SAED pattern indicates several candidate phases. Most contain structural water, e.g., chlorite and talc, and simulated SAED patterns provide reasonable matches to the experimental data. Taking the chemical composition into account, anthophyllite amphibole is the most reasonable candidate phase. We attempted to acquire more SAED patterns in different orientations in order to verify the identification of this grain, but it was not amenable to additional zone-axis orientations.

XANES (Section 2.7) analysis of the GEMS-like glass in the D-rich hotspot of section E1-A (uppermost spectrum, Fig. 7A) shows a strong peak at 290 eV, which is the characteristic absorption energy for carbonate bonding. The spatially correlated detection of minor Ca in the TEM (EDS, Fig. S4) and carbonate by C-XANES implies Ca-bearing carbonate. No large carbonate crystals were observed in the bright-field TEM or HAADF images (Fig. 8B–C). High-resolution TEM (Fig. 8D) imaging reveals discrete nano-crystals (~2 nm) and an SAED pattern shows two diffuse rings (Fig. 8F), which is characteristic of fine-grained material with short-range order. X-ray spectrum imaging shows prominent peaks of Fe, Mg, and Ca in the region where the

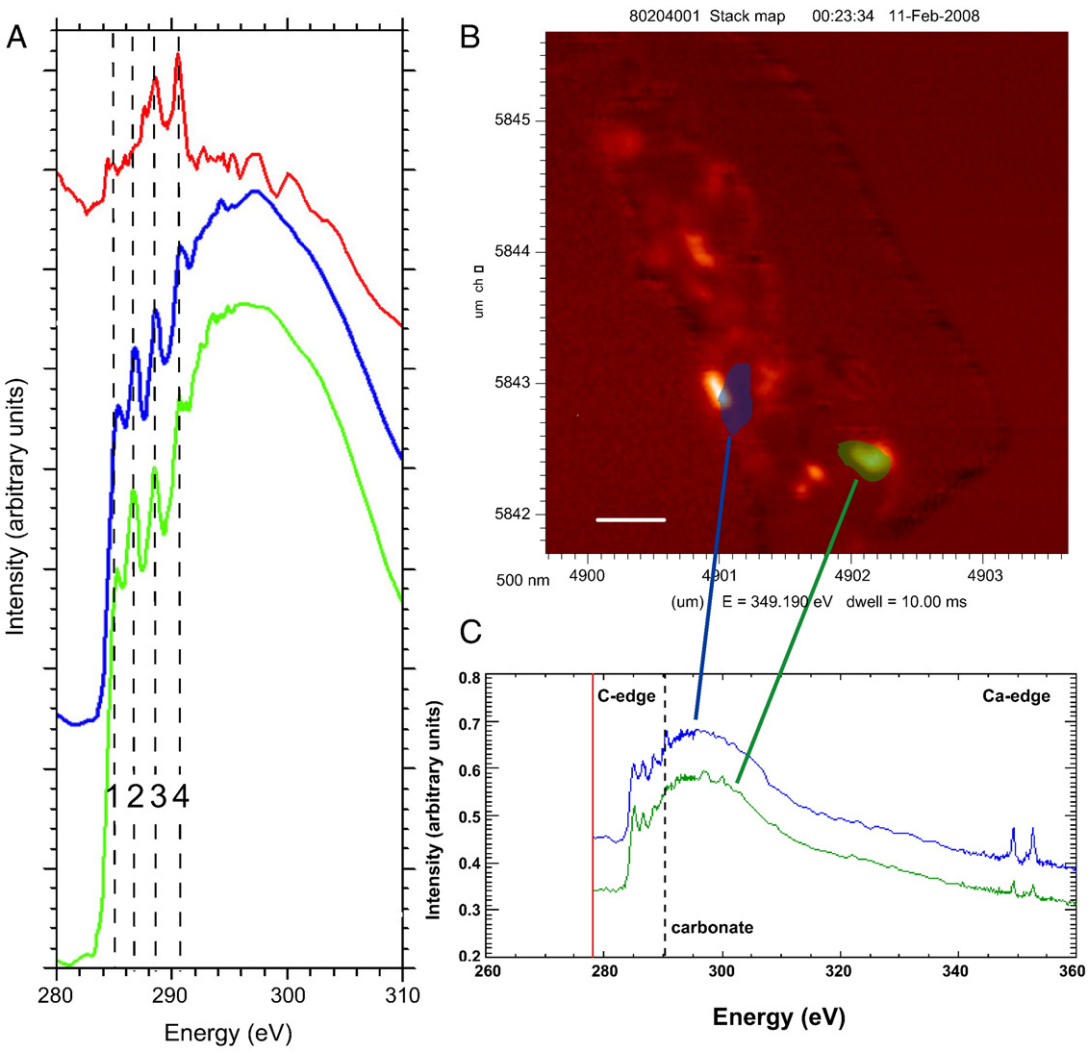

Fig. 7. XANES results of material in GSC-IDPs associated with interstellar organic matter. (A) C-XANES spectra revealed the presence of carbonate bonding by the intense peak at ~290.3 eV (line 4). The OM (red spectrum: D-rich region from section E1-A, Fig. 8, blue spectrum: ^{15}N-rich hotspot from section E1-B, Fig. 4, green spectrum: OM associated with presolar olivine, Fig. 4) is only moderately aromatic and highly oxygenated, evident by the relatively weak absorption at 285 eV (line 1) and the relatively intense absorption at ~286.5 and 288.5 eV (lines 2 and 3), respectively. The intense peak at ~286.5 eV (line 2) most likely indicates vinyl-ketone moieties. (B) XANES Ca-edge absorption map of section E1-B showing the localised distribution of Ca in hotspots measuring tens to hundreds of nm. The bright particularly Ca-rich spots are also rich in S (EDS, not shown). The scale bar is 500 nm. (C) C- and Ca-XANES spectra of selected regions of section E1-B (B) showing that some of the Ca is—as in section E1-A—associated with carbonate as indicated by the intense absorption near 290.3 eV originating from the CO_3 functional group (blue spectrum).

carbonates occur (Fig. S4) and Ca was also detected by Ca-XANES in this region (Fig. 7). Similar patterns originating from particularly small Mg–Fe carbonate (no Ca) have been found in Wild 2 material from the Stardust collection (Mikouchi et al., 2007).

3.5. ^{15}N hotspot in IDP E1

In addition to the presolar olivine associated with a nano-globule (Section 3.2), section E1-B (Fig. 4A) also contains a large ^{15}N anomaly (δ^{15}N ~1300‰, Fig. 1G) that is carried by organic matter. As discussed in Section 3.3, the OM in this section is very pristine, similar to the OM in E1-A, based on the C-XANES detection of functional groups that are not highly aromatic but relatively rich in O. The ^{15}N-rich hotspot is associated with a very fine-grained (nm to tens of nm) mixture of amorphous and crystalline phases, including Mg–Si–O rich glass, silicate crystals, C-rich material and Fe–Ni-sulfides, indicating that this material did not experience any significant processing at elevated temperatures after accretion. STXM data of the whole section show no signs for hydrated silicates, which agrees with IDP E1 being anhydrous. Ca-XANES (Fig. 7B) and EDS spectral imaging prove the localised presence of Ca within the section. C-XANES analysis of the ^{15}N-rich material (Fig. 7A, C) yields the characteristic absorption peak at ~290 eV showing that the OM contains carbonate—similar to the nearby D-rich GEMS-like object.

4. Discussion

4.1. Origin and extremely primitive character of the GSC-IDPs

The isotopic compositions and disordered nature of the organic matter, presolar-grain abundances and distribution, and textures of the studied GSC-IDPs, especially the cluster fragment E1 and the individual IDP G4 render them among the most primitive extraterrestrial materials yet identified. While many primitive characteristics have been found already in various IDPs (e.g., Keller et al., 2000; Messenger, 2000; Flynn et al., 2003; Floss et al., 2004; Messenger et al., 2005; Floss et al., 2006) the accumulation of all these properties within two IDPs lets us argue that these are indeed “ultra-primitive”, standing out of the background flux of pristine but otherwise relatively common IDPs. It also appears that cluster IDPs are not necessarily more primitive than individual IDPs.

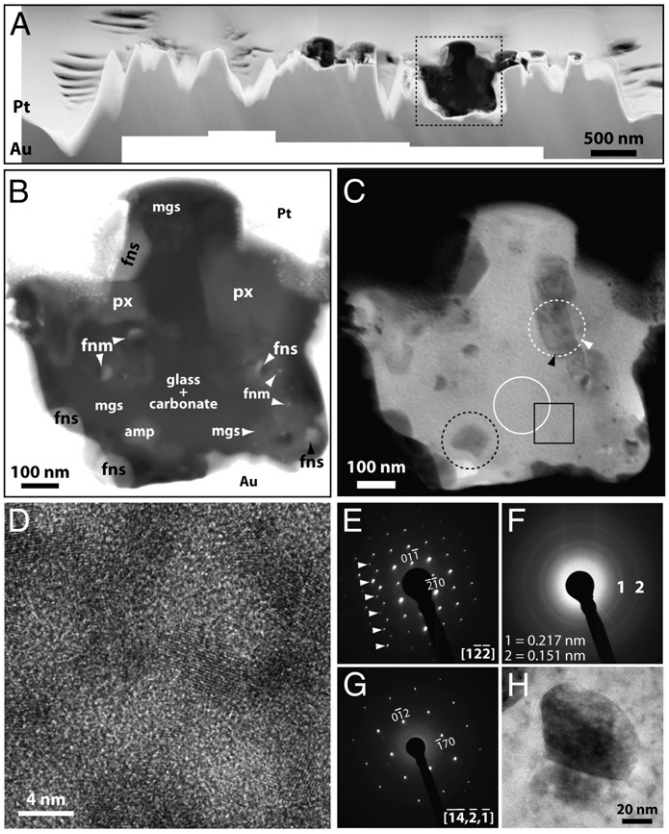

Fig. 8. TEM data on section E1-A. (A) HAADF image showing the overall section with the IDP sandwiched between Pt strap and Au foil. A presolar silicate near the right end of the section (#8, Fig. 2A) was apparently completely consumed by the SIMS measurement prior to FIB lift-out. (B) HAADF image of D hotspot (Fig. 1) indicated by the dashed rectangle in (A) reveals the fine-grained character of this GEMS-like aggregate. Magnesium silicate (mgs), pyroxene (px), Fe–Ni metal (fnm), Fe–Ni sulfide (fns), and amphibole (amp) occur with glass and carbonate. (C) Bright-field image of the same area as (B). (D) HRTEM image of the region enclosed by the black square in (C), revealing ~4 nm wide nano-crystalline carbonate grains surrounded by amorphous material. (E) SAED pattern acquired from the area enclosed by the white-dashed circle in (C). Two sets of reflections occur in the pattern, indicating that the pyroxene grain is polycrystalline. The primary set of reflections comes from the grain showing dark diffraction contrast indicated by the black arrowhead in (C). The other set of reflections (white arrowheads) originates from the material between the right-most edge of the grain and the circle in (C) indicated by the white arrowhead. (F) SAED pattern acquired from the area enclosed by the solid-white circle in (C). The pattern contains two diffuse rings, consistent with nano-crystalline grains containing short-range order. Measurements of the d-spacings (inset), are consistent with carbonate. (G) SAED pattern acquired from the grain enclosed by the black-dashed circle in (C) indexed to amphibole. (H) Bright-field image of the amphibole grain rotated ~90° clockwise relative to (C).

Moreover, the close similarity of E1 and G4 suggests that they have a common origin despite being found on different parts of an IDP collector that flew for 7.9 h through the stratosphere.

The observation of four ^{17}O-depleted grains in a single ~5 μm IDP (G4) is particularly remarkable, given that such grains make up at maximum ~5% of the meteoritic presolar grain inventory (Nittler et al., 1997). A similar clustering has been seen in a 20 μm × 20 μm sized sub-region of an Antarctic micrometeorite, in which five of the rare Group 4 grains were identified (Yada et al., 2008). However, because the analyzed area of G4 is only ~70 μm^2, the presolar grain abundance is much higher in this IDP. The presence of "clusters" of two different presolar grain types, one being particularly rare, in E1 and G4 (Figs. 2 and 3), and also the close spatial association of the presolar olivine with interstellar OM (Fig. 4A) suggest that these GSC-IDPs sample reservoirs of presolar and primitive materials were less homogenized in the early solar system than those that produced the asteroidal parent bodies of meteorites. The GSC-IDPs may contain small assemblages of relict interstellar material.

Other analyses of IDPs collected during the Earth's passage through the Grigg–Skjellerup dust trail have revealed additional unusual properties: (i) perhaps most important, noble gases that imply extraordinarily short free transfer times after ejection (Palma et al., 2005), (ii) a previously unknown manganese-silicide phase ("Brownleeite", Nakamura-Messenger et al., 2008), and (iii) the presence of an unknown, isotopically "exotic" ^{3}He-rich and ^{22}Ne-poor component (Palma et al., 2005).

The culmination of exceptional observations on this subset of IDPs from NASA collectors L2054, L2055, and U2121 coincide with their specific collection history, leading us to infer that these particles may indeed originate from comet Grigg–Skjellerup. The enhanced probability for collecting fresh dust from this comet inferred by Messenger (2002) is the only parameter that was different from the dust collection in previous periods. Hence, the two most primitive IDPs likely sample—as do the Stardust samples from comet Wild 2—a known JFC.

4.2. Molecular cloud organic matter

Mechanisms within the solar system that are capable of enriching OM in D and ^{15}N to the extreme values found here in the GSC-IDPs (Section 3.3) and in IDPs in general are unknown. This implies an origin for the OM in the interstellar medium or, perhaps, outer reaches of the protoplanetary disk, where low-temperature chemical reactions are suggested to have produced such enrichments (Millar et al., 1989; Messenger, 2000; Messenger et al., 2003b; Charnley and Rodgers, 2008a,b). We favour an interstellar origin because the OM was well mixed throughout the early solar system (Alexander et al., in preparation, see also next paragraph). While enrichments in ^{15}N in OM could, in principle, be of stellar nucleosynthetic origin, D is burnt to ^{3}He at the earliest stage of stellar evolution, causing the outflowing material in later stages to be D-poor, which excludes that the D- and ^{15}N-rich OM is of stellar origin.

Organic matter in the most primitive meteorites also shows micron-scale heterogeneity (Busemann et al., 2006a) with *D*/*H* and ^{15}N/^{14}N values comparable to those observed here for the GSC-IDPs. Hence, a similar assemblage of interstellar OM has apparently been incorporated in the parent bodies of IDPs and meteorites, although these planetary bodies were formed in distinct regions of the solar system. This observation supports general turbulent radial mixing scenarios suggested for the early solar system (as does the presence of high-temperature materials in the outer solar system, as found in Stardust, Brownlee et al., 2006), and particularly the inward transport of material (e.g., Ciesla, 2009 and references therein). The interstellar organic matter in primitive meteorites (Busemann et al., 2006a; Alexander et al., 2007a) must have been stored, protected from high temperatures, outside the meteorite-forming regions prior to accretion into meteorite parent bodies. Temperatures necessary to anneal most of the amorphous interstellar silicates in the inner solar system (>1000 K, Alexander et al., 2007b) would have destroyed the organic matter and equilibrated the D and ^{15}N-rich hotspots.

4.3. Similarities and diversity among JFCs

Accepting the hypothesis that a fraction of the examined GSC-IDPs are indeed from Grigg–Skjellerup (see Section 4.1, acknowledging that this is not proven, but inferred based on extreme laboratory findings coinciding with the collection history) allows us to compare three distinctively examined JFCs: Grigg–Skjellerup, Wild 2 and Tempel 1, which was spectroscopically analyzed during the Deep Impact experiment (A'Hearn et al., 2005; Lisse et al., 2006). All three contain a mixture of (i) matter that is expected in outer solar system bodies, including pristine, amorphous carbon and volatile-rich matter, and (ii) refractory minerals with high-temperature inner solar system origin, such as olivines and Ca-rich minerals (Brownlee et al., 2006; Ishii et al., 2008; Wooden, 2008). Moreover, and somewhat surprising,

carbonates (and perhaps hydrated silicates, Rotundi et al., 2008) appear to be present in all three (Lisse et al., 2006; Mikouchi et al., 2007; Flynn et al., 2008).

Thus, our identification of carbonates and hydrated silicates (e.g., the occurrence of amphibole, Section 3.4) in nominally anhydrous IDPs is unusual, but not unprecedented (e.g., Rietmeijer, 1990; Nakamura et al., 2005; Flynn et al., 2008). A number of scenarios have been proposed to explain their presence (e.g., Rietmeijer, 1985, 2002; Wooden, 2008), not all of them requiring parent-body alteration by liquid water. For example, both experiments (Toppani et al., 2005) and astronomical observations (Kemper et al., 2002) support the possibility of direct condensation of carbonates.

The basic agreement in the components of the three comets is remarkable, suggesting that JFCs may have generally sampled—at large scales—a similar mixture of materials during their formation 4.56 Gyr ago. We do, however, also observe differences in the two sample sets available for laboratory analysis, where a more detailed examination including isotopic considerations is possible. The as-yet analyzed Wild 2 dust is clearly less primitive than the GSC-IDPs: observed D enrichments in Wild 2 samples reach only modest values ($\leq \delta D$ ~1000‰, McKeegan et al., 2006), presolar grains are rare (McKeegan et al., 2006; Stadermann and Floss, 2008; Messenger et al., 2009), and Raman spectroscopy (Sandford et al., 2006; Rotundi et al., 2008) indicates more thermal processing of most of the organics in Wild 2 than in the GSC-IDPs. Yet, distinct primitive features were—so far rarely—recognized in Wild 2 dust too, such as a very labile organic component rich in N and O relative to C and meteoritic OM (Sandford et al., 2006; Cody et al., 2008), OM enriched in ^{15}N (Sandford et al., 2006), primordial noble gases (Marty et al., 2008), and most recently, nano-globules (De Gregorio et al., 2009).

Thus, at least some Wild 2 dust was not significantly altered during impact, but comparing both sets of JFC material is nevertheless complex due to potential sampling bias. For example, it is possible that Wild 2 analyses have largely discriminated against the most primitive material. Although much attention has been paid to "terminal particles" at the end of the aerogel tracks, the "bulbous" upper-track regions (Brownlee et al., 2006) may have formed by fragmentation on impact of more fragile material, perhaps more similar to the fine-grained GSC-IDPs. The average pre-impact density of the Wild 2 dust that caused the bulbous track features in the Stardust aerogel collectors is debated. It might have been as low as ~1 g/cm^3. However, the comparison with impact experiments suggests only a few low-density impactors and an average density for Wild 2 particles of ~2.4 g/cm^3 in poorly consolidated aggregates (Kearsley et al., 2009). Hence, some Wild 2 dust could be more similar either to porous IDPs or to chondritic matrix, rather than to the more refractory siliceous material from the inner solar system. Abundant porous dust aggregates at the >10 wt.% level were inferred for the periodic comet Halley coma (Lasue et al., 2009). Conversely, in addition to selection bias during curation, IDPs may reflect a natural bias, favouring the most primitive materials: "fluffy" low-density cometary IDPs survive the deceleration in the upper most atmosphere best, whereas denser particles experience more severe heating (Levasseur-Regourd et al., 2006).

The conventional wisdom of a sharp distinction between processed, high-temperature materials in the inner solar system and unprocessed, primitive matter in the outer solar system was first overturned by observations of crystalline silicates in comets (Campins and Ryan, 1989; Wooden, 2008). Moreover, a number of evolutionary mechanisms have been identified that could affect comets over the history of the solar system (Stern, 2003). Observations from the Wild 2 samples (Ishii et al., 2008) argue further against this strict dichotomy, indicating "asteroid-like" material in comet dust. In addition, the cometary dust described herein also contains assemblages of unequalled, largely unprocessed interstellar material. Therefore, it appears that JFCs are extremely heterogeneous at a (sub-) micrometer-scale, while at a cometary scale the observations show similar major components in various JFCs. It is important to note here that—owing to the limited sample sets available (e.g., ~1 mg comet Wild 2 dust and orders of magnitude less from all IDPs combined)—the possibility for heterogeneity within each comet nucleus, maybe at an intermediate scale, cannot be excluded.

Further macroscopic differences between JFCs have been observed, such as depletions in carbon-chain molecules among JFCs, including Wild 2 (A'Hearn et al., 1995), compositional differences of the ices, indicating formation in distinct heliocentric distances (DiSanti and Mumma, 2008), and dust mass distributions (Green et al., 2004). These observations are consistent with incomplete large-scale mixing of matter in the early outer solar system that formed the icy objects in the Edgeworth–Kuiper-belt or scattered disk, or, maybe, with the provenance of some JFCs in the Oort cloud (A'Hearn et al., 1995; DiSanti and Mumma, 2008). It will be essential to analyze remnants of the most fragile components of Wild 2 dust trapped in the uppermost regions of the Stardust tracks, and the most refractory available fragments of Grigg–Skjellerup dust at the micrometer-scale in the laboratory to fully assess the true primordial diversity of JFCs.

4.4. Comparisons with cometary dust from Halley

The JFC dust can also be compared with results obtained from short-period (75.3 yr) comet 1P/Halley dust, examined onboard the Giotto and Vega 1 and 2 spacecrafts (e.g., Kissel et al., 1986a,b; Fomenkova, et al., 1992; Jessberger, 1999). Halley is not a JFC, but most likely deflected from a long-period orbit and originated in the Oort cloud (e.g., DiSanti and Mumma, 2008) or, perhaps, in the scattered (Kuiper) disk (Levison et al., 2006). The Giotto and Vega observations were the first that allowed in-situ examinations of cometary dust from a known source. These observations show that the similarities and differences found here for three JFCs might be extended to all outer solar system reservoirs of cometary matter: (i) generally, the components of the IDPs cover the range between endmember components found in Halley dust; the widespread refractory organic material, rich in H, C, N and O ("CHON", Jessberger, 1999, and references therein), and grains made mainly of rock-forming elements such as Mg, Si and Fe (Fomenkova et al., 1992). The average CHON composition ($C_{100}H_{80}N_4O_{20}S_2$, Kissel and Krueger, 1987) closely matches the nominal composition of meteoritic insoluble organic matter (Alexander et al., 2007a). (ii) The "rocky" material is coated with the organic component, as observed also for IDPs (Kissel and Krueger, 1987, Jessberger, 1999). (iii) CHON and the rocky component are fluffy and of low density, similar to IDPs (e.g., Kissel and Krueger, 1987). (iv) The rocky material contains metals, Mg-rich silicates and sulfides, thus resembling the primary mineralogy found in IDPs and Wild 2 samples (Schulze et al., 1997; Jessberger, 1999). (v) Mg-rich dust analyzed onboard the VEGA spacecraft may include carbonates (Fomenkova et al., 1992).

All these observations are similar to those for JFC dust, suggesting that the same mixture of primitive matter has been incorporated into cometary objects of different origin. However, as with the differences found among JFCs, some observations on Halley dust support the idea of heterogeneity, either between comets, or simply within each comet at the examined micrometer scale: carbon in the Halley dust appears to be generally isotopically light with ratios approaching ^{12}C/^{13}C ~5000 and refractory, CAI-type material has not been detected (Jessberger, 1999 and references therein). In contrast, the range of C isotopic compositions measured in organic matter in both the GSC-IDPs and in Wild 2 dust is relatively small (typically ±10% around terrestrial values).

5. Conclusions

1. Two of the anhydrous chondritic porous interplanetary dust particles analyzed here from NASA collector L2054 flown through the dust stream of comet Grigg–Skjellerup contain some of the most primitive materials analyzed as yet in the laboratory.
2. The organic matter shows among the largest enrichments in D and ^{15}N of all IDPs proving the presence of extremely pristine organic

matter, most likely originating in the Sun's progenitor molecular cloud. Raman spectroscopy reveals particularly disordered carbon, indicating that the IDPs did not experience any significant thermal alteration. Presolar-grain abundances are extremely high. One IDP carries four ^{17}O-depleted grains of the particularly rare Group 3, possibly originating from supernovae (Nittler et al., 2008).

3. TEM shows that one of the presolar Group 1 red giant star grains is a Ca-bearing Mg-rich olivine. This grain is closely associated with an organic nano-globule of most likely interstellar origin (Nakamura-Messenger et al., 2006).
4. These observations indicate that the IDPs contain significant amounts (at the percent level) of interstellar assemblages that survived accretion and evolution of the solar system. This supports the suggestion (Bradley, 2003) that the most primitive anhydrous IDPs may originate from comets, where protoplanetary cloud material will survive best (Charnley and Rodgers, 2008a).
5. The particularly primitive character of these IDPs collected during April 2003 coincides with the prediction (Messenger, 2002) of an enhanced flux of dust particles originating from comet 26P/Grigg–Skjellerup during this period. This leads us to suggest that dust from this Jupiter-family comet (JFC) is indeed among the IDPs from collector L2054. This allows a comparison with JFCs 81P/Wild 2 and 9P/Tempel 1.
6. The presence of carbonate and amphibole in nominally anhydrous IDPs agrees with observations of carbonates in comet Wild 2 dust (Mikouchi et al., 2007) and comet Tempel 1 (Lisse et al., 2006). This emphasizes the possibility of widespread formation of these minerals without the presence of liquid water in protoplanetary environments (Kemper et al., 2002; Toppani et al., 2005).
7. Differences (Ishii et al., 2008) observed between cometary samples so far available in the laboratory, i.e., IDPs and Wild 2 Stardust, might largely be explainable by alteration during collection in aerogel, (curational) sampling bias, and natural selection during atmospheric entry.
8. The organic matter in IDPs and the most primitive meteorites (Busemann et al., 2006a) are very similar, implying large radial mixing including significant inward transport (e.g., Ciesla, 2009).
9. The study of a large number of IDPs collected in dedicated campaigns during enhanced cometary dust flux activity might provide an inexpensive additional path to detect cometary material from specific comets in order to better understand their properties and origins.

Acknowledgements

This work was supported by NASA's Cosmochemistry (NNG004GF61G) and Origins of the Solar System (NNX07AJ71G) programmes (L.R.N.), by the NASA Astrobiology Institute, the Office of Naval Research and by the Director, Office of Science, Office of Basic Energy Sciences, of the U.S. Department of Energy under Contract No. DE-AC02-05CH11231. Constructive and helpful comments by two anonymous reviewers are much appreciated. We thank C. M. O'D. Alexander and S. F. Green for discussions, the NASA Astromaterials Acquisition and Curation Centre for providing the IDPs, and M. Fries and A. Steele for support with the Raman spectroscopy.

Appendix A. Supplementary data

Supplementary data associated with this article can be found, in the online version, at doi:10.1016/j.epsl.2009.09.007.

References

A'Hearn, M.F., Belton, M.J.S., Delamere, W.A., Kissel, J., Klaasen, K.P., McFadden, L.A., Meech, K.J., Melosh, H.J., Schultz, P.H., Sunshine, J.M., Thomas, P.C., Veverka, J., Yeomans, D.K., Baca, M.W., Busko, I., Crockett, C.J., Collins, S.M., Desnoyer, M., Eberhardy, C.A., Ernst, C.M., Farnham, T.L., Feaga, L., Groussin, O., Hampton, D., Ipatov, S.I., Li, J.-Y., Lindler, D., Lisse, C.M., Mastrodemos, N., Owen Jr., W.M., Richardson, J.E., Wellnitz, D.D., White, R.L., 2005. Deep Impact: excavating comet Tempel 1. Science 310, 258–264.

A'Hearn, M.F., Millis, R.L., Schleicher, D.G., Osip, D.J., Birch, P.V., 1995. The ensemble properties of comets: results from narrowband photometry of 85 comets, 1976–1992. Icarus 118, 223–270.

Aléon, J., Engrand, C., Robert, F., Chaussidon, M., 2001. Clues to the origin of interplanetary dust particles from the isotopic study of their hydrogen-bearing phases. Geochim. Cosmochim. Acta 65, 4399–4412.

Aléon, J., Robert, F., Chaussidon, M., Marty, B., 2003. Nitrogen isotopic composition of macromolecular organic matter in interplanetary dust particles. Geochim. Cosmochim. Acta 67, 3773–3783.

Alexander, C.M.O'D., 1993. Presolar SiC in chondrites: how variable and how many sources? Geochim. Cosmochim. Acta 57, 2869–2888.

Alexander, C.M.O'D., Fogel, M., Yabuta, H., Cody, G.D., 2007a. The origin and evolution of chondrites recorded in the elemental and isotopic compositions of their macromolecular organic matter. Geochim. Cosmochim. Acta 71, 4380–4403.

Alexander, C.M.O'D., Boss, A.P., Keller, L.P., Nuth, J.A., Weinberger, A., 2007b. Astronomical and meteoritic evidence for the nature of interstellar dust and its processing in protoplanetary disks. In: Reipurth, B., Jewitt, D., Keil, K. (Eds.), Protostars and Planets V. University of Arizona Press, Tucson, pp. 801–813.

Alexander, C.M.O'D., Cody, G., Yabuta, H., Busemann, H., Nittler, L.R., Stroud, R.M., Zega, T., de Gregorio, B., Martins, Z., in preparation. The central importance of organic matter to understanding the origin and early evolution of the Solar System. Chem. Erde.

Bradley, J.P., 2003. Interplanetary dust particles. In: Davies, A.M. (Ed.), Treatise on Geochemistry—Vol. 1 Meteorites, Comets, and Planets. Elsevier, pp. 689–711.

Bradley, J.P., Keller, L.P., Snow, T.P., Hanner, M.S., Flynn, G.J., Gezo, J.C., Clemett, S.J., Brownlee, D.E., Bowey, J.E., 1999. An infrared spectral match between GEMS and interstellar grains. Science 285, 1716–1718.

Brownlee, D.E., Joswiak, D.J., Schlutter, D.J., Pepin, R.O., Bradley, J.P., Love, S.G., 1995. Identification of individual cometary IDP's by thermally stepped He release. Lunar Planet. Sci. Conf. XXVI, 183–184.

Brownlee, D., Tsou, P., Aléon, J., Alexander, C.M.O'D., Araki, T., Bajt, S., Baratta, G.A., Bastien, R., Bland, P., Bleuet, P., Borg, J., Bradley, J.P., Brearley, A., Brenker, F., Brennan, S., Bridges, J.C., Browning, N., Brucato, J.R., Brucato, H., Bullock, E., Burchell, M.J., Busemann, H., Butterworth, A., Chaussidon, M., Cheuvront, A., Chi, M., Cintala, M.J., Clark, B.C., Clemett, S.J., Cody, G., Colangeli, L., Cooper, G., Cordier, P., Daghlian, C., Dai, Z., D'Hendecourt, L., Djouadi, Z., Dominguez, G., Duxbury, T., Dworkin, J.P., Ebel, D., Economou, T.E., Fairey, S.A.J., Fallon, S., Ferrini, G., Ferroir, T., Fleckenstein, H., Floss, C., Flynn, G., Franchi, I.A., Fries, M., Gainsforth, Z., Gallien, J.-P., Genge, M., Gilles, M.K., Gillet, P., Gilmour, J., Glavin, D.P., Gounelle, M., Grady, M.M., Graham, G.A., Grant, P.G., Green, S.F., Grossemy, F., Grossman, L., Grossman, J., Guan, Y., Hagiya, K., Harvey, R., Heck, P., Herzog, G.F., Hoppe, P., Hörz, F., Huth, J., Hutcheon, I.D., Ishii, H., Ito, M., Jacob, D., Jacobsen, C., Jacobsen, S., Joswiak, D., Kearsley, A.T., Keller, L., Khodja, H., Kilcoyne, A.L.D., Kissel, J., Krot, A., Langenhorst, F., Lanzirotti, A., Le, L., Leshin, L., Leitner, J., Lemelle, L., Leroux, H., Liu, M.-C., Luening, K., Lyon, I., MacPherson, G., Marcus, M.A., Marhas, K., Matrajt, G., Meibom, A., Mennella, V., Messenger, K., Mikouchi, T., Mostefaoui, S., Nakamura, T., Nakano, T., Newville, M., Nittler, L.R., Ohnishi, I., Ohsumi, K., Okudaira, K., Papanastassiou, D.A., Palma, R., Palumbo, M.E., Pepin, R.O., Perkins, D., Perronnet, M., Pianetta, P., Rao, W., Rietmeijer, F., Robert, F., Rost, D., Rotundi, A., Ryan, R., Sandford, S.A., Schwandt, C.S., See, T.H., Schlutter, D., Sheffield-Parker, J., Simionovici, A., Simon, S., Sitnitsky, I., Snead, C.J., Spencer, M.K., Stadermann, F.J., Steele, A., Stephan, T., Stroud, R., Susini, J., Sutton, S.R., Taheri, M., Taylor, S., Teslich, N., Tomeoka, K., Tomioka, N., Toppani, A., Trigo-Rodríguez, J.M., Troadec, D., Tsuchiyama, A., Tuzolino, A.J., Tyliszczak, T., Uesugi, K., Velbel, M., Vellenga, J., Vicenzi, E., Vincze, L., Warren, J., Weber, I., Weisberg, M., Westphal, A.J., Wirick, S., Wooden, D., Wopenka, B., Wozniakiewicz, P., Wright, I., Yabuta, H., Yano, H., Young, E.D., Zare, R.N., Zega, T., Ziegler, K., Zimmerman, L., Zinner, E., Zolensky, M., 2006. Comet 81P/Wild 2 under a microscope. Science 314, 1711–1716.

Busemann, H., Young, A.F., Alexander, C.M.O'D., Hoppe, P., Mukhopadhyay, S., Nittler, L.R., 2006a. Interstellar chemistry recorded in organic matter from primitive meteorites. Science 312, 727–730.

Busemann, H., Alexander, C.M.O'D., Nittler, L.R., Zega, T.J., Stroud, R.M., Bajt, S., Cody, G.D., Yabuta, H., 2006b. Correlated analyses of D- and ^{15}N-rich carbon grains from CR2 chondrite EET 92042. Meteorit. Planet. Sci. 41, A34.

Busemann, H., Alexander, C.M.O'D., Nittler, L.R., 2007. Characterization of insoluble organic matter in primitive meteorites by micro-Raman spectroscopy. Meteorit. Planet. Sci. 42, 1387–1416.

Busemann, H., Nittler, L.R., Davidson, J., Franchi, I.A., Messenger, S., Nakamura-Messenger, K., Palma, R.L., Pepin, R.O., 2009. Carbon Raman spectroscopy of 36 interplanetary dust particles. Meteorit. Planet. Sci. 44 abstract No. 5412.

Campins, H., Ryan, E.V., 1989. The identification of crystalline olivine in cometary silicates. Astrophys. J. 341, 1059–1066.

Charnley, S.B., Rodgers, S.D., 2008a. Interstellar reservoirs of cometary matter. Space Sci. Rev. 138, 59–73.

Charnley, S.B., Rodgers, S.D., 2008b. Nitrogen superfractionation in interstellar chemistry. Lunar Planet. Sci. Conf. XXXIX, 2233.

Ciesla, F.J., 2009. Two-dimensional transport of solids in viscous protoplanetary disks. Icarus 200, 655–671.

Cody, G.D., Alexander, C.M.O'D., 2005. NMR studies of chemical structural variation of insoluble organic matter from different carbonaceous chondrite groups. Geochim. Cosmochim. Acta 69, 1085–1097.

Cody, G.D., Ade, H., Alexander, C.M.O'D., Araki, T., Butterworth, A., Fleckenstein, H., Flynn, G., Gilles, M.K., Jacobsen, C., Kilcoyne, A.L.D., Messenger, K., Sandford, S.A., Tyliszczak, T., Westphal, A.J., Wirick, S., Yabuta, H., 2008. Quantitative organic and light-element analysis of comet 81P/Wild 2 particles using C-, N-, and O- μ-XANES. Meteorit. Planet. Sci. 43, 353–365.

De Gregorio, B.T., Stroud, R.M., Nittler, L.R., Cody, G.D., Kilcoyne, A.L.D., 2009. Isotopically anomalous organic globules from comet 81P/Wild 2. Lunar Planet. Sci. Conf. XXXX, 1130.

DiSanti, M.A., Mumma, M.J., 2008. Reservoirs for comets: compositional differences based on infrared observations. Space Sci. Rev. 138, 127–145.
Floss, C., Stadermann, F., 2008. The stardust inventories of CR chondrites QUE 99177 and MET 00426, and the distribution of presolar silicate and oxide grains in the early solar system. Lunar Planet. Sci. Conf. XXXIX, 1280.
Floss, C., Stadermann, F., 2009. Auger nanoprobe analysis of presolar ferromagnesian silicate grains from primitive CR chondrites QUE 99177 and MET 00426. Geochim. Cosmochim. Acta 73, 2415–2440.
Floss, C., Stadermann, F.J., Bradley, J., Dai, Z.R., Bajt, S., Graham, G., 2004. Carbon and nitrogen isotopic anomalies in an anhydrous interplanetary dust particle. Science 303, 1355–1358.
Floss, C., Stadermann, F.J., Bradley, J.P., Dai, Z.R., Bajt, S., Graham, G., Lea, A.S., 2006. Identification of isotopically primitive interplanetary dust particles: a NanoSIMS isotopic imaging study. Geochim. Cosmochim. Acta 70, 2371–2399.
Flynn, G.J., Keller, L.P., Feser, M., Wirick, S., Jacobsen, C., 2003. The origin of organic matter in the solar system: evidence from the interplanetary dust particles. Geochim. Cosmochim. Acta 67, 4791–4806.
Flynn, G.J., Leroux, H., Tomeoka, K., Tomioka, N., Ohnishi, I., Mikouchi, T., Wirick, S., Keller, L.P., Jacobsen, C., Sandford, S.A., 2008. Carbonate in comets: a comparison of comets 1P/Halley, 9P/Temple 1, and 81P/Wild 2. Lunar Planet. Sci. Conf. XXXIX, 1391.
Fomenkova, M.N., Kerridge, J.F., Marti, K., McFadden, L.-A., 1992. Compositional trends in rock-forming elements of comet Halley dust. Science 258, 266–269.
Garvie, L.A.J., Baumgardner, G., Buseck, P.R., 2008. Scanning electron microscopical and cross sectional analysis of extraterrestrial carbonaceous nanoglobules. Meteorit. Planet. Sci. 43, 899–903.
Green, S.F., McDonnell, J.A.M., McBride, N., Colwell, M.T.S.H., Tuzzolino, A.J., Economou, T.E., Tsou, P., Clark, B.C., Brownlee, D.E., 2004. The dust mass distribution of comet 81P//Wild 2. J. Geophys. Res. - E 109. doi:10.1029/2004JE002318.
Hoppe, P., Ott, U., Lugmair, G.W., 2004. NanoSIMS, the new tool of choice: ^{26}Al, ^{44}Ti, ^{49}V, ^{53}Mn, ^{60}Fe, and more. New Astron. Rev. 48, 171–176.
Hoppe, P., Leitner, J., Meyer, B.S., The, L.-S., Lugaro, M., Amari, S., 2009. An unusual presolar silicon carbide grain from a supernova: implications for the production of silicon-29 in type II supernovae. Astrophys. J. 691, L20–L23.
Hovmöller, S., 1992. CRISP: crystallographic image processing on a personal computer. Ultramicroscopy 41, 121–135.
Ishii, H.A., Bradley, J.P., Dai, Z.R., Chi, M., Kearsley, A.T., Burchell, M.J., Browning, N.D., Molster, F., 2008. Comparison of Comet 81P/Wild 2 dust with interplanetary dust from comets. Science 319, 447–450.
Jessberger, E.K., 1999. Rocky cometary particulates: their elemental, isotopic and mineralogical ingredients. Space Sci. Rev. 90, 91–97.
Kearsley, A.T., Burchell, M.J., Price, M.C., Graham, G.A., Cole, M.J., 2009. Porous aggregates in comet 81P/Wild 2? Stardust Al foil craters compared to experimental impacts from artificial aggregates and meteorite powders. Lunar Planet. Sci. Conf. XXXX, 1517.
Keller, L.P., Messenger, S., 2004. On the origin of GEMS. Lunar Planet. Sci. Conf. XXXV, 1985.
Keller, L.P., Messenger, S., 2008. Coordinated chemical and isotopic studies of GEMS grains in IDPs. Lunar Planet. Sci. Conf. XXXIX, 2347.
Keller, L.P., Messenger, S., Bradley, J.P., 2000. Analysis of a deuterium-rich interplanetary dust particle (IDP) and implications for presolar material in IDPs. J. Geophys. Res. 105, 10397–10402.
Keller, L.P., Messenger, S., Flynn, G.J., Clemett, S., Wirick, S., Jacobsen, C., 2004. The nature of molecular cloud material in interplanetary dust. Geochim. Cosmochim. Acta 68, 2577–2589.
Kemper, F., Jäger, C., Waters, L.B.F.M., Henning, T., Molster, F.J., Barlow, M.J., Lim, T., de Koter, A., 2002. Detection of carbonates in dust shells around evolved stars. Nature 415, 295–297.
Kilcoyne, A.L.D., Tyliszczak, T., Steele, W.F., Fakra, S., Hitchcock, P., Franck, K., Anderson, E., Harteneck, B., Rightor, E.G., Mitchell, G.E., Hitchcock, A.P., Yang, L., Warwick, T., Ade, H., 2003. Interferometer-controlled scanning transmission x-ray microscopes at the Advanced Light Source. J. Synchrotron Radiat. 10, 125–136.
Kissel, J., Krueger, F.R., 1987. The organic component in dust from comet Halley as measured by the PUMA mass spectrometer on board Vega 1. Nature 326, 755–760.
Kissel, J., Sagdeev, R.Z., Bertaux, J.L., Angarov, V.N., Audouze, J., Blamont, J.E., Büchler, K., Evlanov, E.N., Fechtig, H., Fomenkova, M.N., von Hoerner, H., Inogamov, N.A., Khromov, V.N., Knabe, W., Krueger, F.R., Langevin, Y., Leonas, V.B., Levasseur-Regourd, A.C., Managadze, G.G., Podkolzin, S.N., Shapiro, V.D., Tabaldyev, S.R., Zubkov, B.V., 1986a. Composition of comet Halley dust particles from Vega observations. Nature 321, 280–282.
Kissel, J., Brownlee, D.E., Büchler, K., Clark, B.C., Fechtig, H., Grün, E., Hornung, K., Igenbergs, E.B., Jessberger, E.K., Krueger, F.R., Kuczera, H., McDonnell, J.A.M., Morfill, G.M., Rahe, J., Schwehm, G.H., Sekanina, Z., Utterback, N.G., Völk, H.J., Zook, H.A., 1986b. Composition of comet Halley dust particles from Giotto observations. Nature 321, 336–337.
Kresák, L., 1987. The 1808 apparition and the long-term physical evolution of periodic comet Grigg–Skjellerup. Bull. Astron. Inst. Czechoslov. 38, 65–75.
Lasue, J., Levasseur-Regourd, A.C., Hadamcik, E., Alcouffe, G., 2009. Cometary dust properties retrieved from polarization observations: application to C/1995 O1 Hale–Bopp and 1P/Halley. Icarus 199, 129–144.
Levasseur-Regourd, A.C., Lasue, J., Desvoivres, E., 2006. Early inner solar system impactors: physical properties of comet nuclei and dust particles revisited. Orig. Life Evol. Biosph. 36, 507–514.
Levison, H.F., Duncan, M.J., Dones, L., Gladman, B.J., 2006. The scattered disk as a source of Halley-type comets. Icarus 184, 619–633.
Lisse, C.M., VanCleve, J., Adams, A.C., A'Hearn, M.F., Fernández, Y.R., Farnham, T.L., Armus, L., Grillmair, C.J., Ingalls, J., Belton, M.J.S., Groussin, O., McFadden, L.A., Meech, K.J., Schultz, P.H., Clark, B.C., Feaga, L.M., Sunshine, J.M., 2006. Spitzer spectral observations of the Deep Impact ejecta. Science 313, 635–640.
Marty, B., Palma, R.L., Pepin, R.O., Zimmermann, L., Schlutter, D.J., Burnard, P.G., Westphal, A.J., Snead, C.J., Bajt, S., Becker, R.H., Simones, J.E., 2008. Helium and neon abundances and compositions in cometary matter. Science 319, 75–78.
McKeegan, K.D., Aléon, J., Bradley, J., Brownlee, D., Busemann, H., Butterworth, A., Chaussidon, M., Fallon, S., Floss, C., Gilmour, J., Gounelle, M., Graham, G., Guan, Y., Heck, P.R., Hoppe, P., Hutcheon, I.D., Huth, J., Ishii, H., Ito, M., Jacobsen, S.B., Kearsley, A., Leshin, L.A., Liu, M.-C., Lyon, I., Marhas, K., Marty, B., Matrajt, G., Meibom, A., Messenger, S., Mostefaoui, S., Mukhopadhyay, S., Nakamura-Messenger, K., Nittler, L., Palma, R., Pepin, R.O., Papanastassiou, D.A., Robert, F., Schlutter, D., Snead, C.J., Stadermann, F.J., Stroud, R., Tsou, P., Westphal, A., Young, E.D., Ziegler, K., Zimmerman, L., Zinner, E., 2006. Isotopic compositions of cometary matter returned by Stardust. Science 314, 1724–1728.
Messenger, S., 2000. Identification of molecular-cloud material in interplanetary dust particles. Nature 404, 968–971.
Messenger, S., 2002. Opportunities for the stratospheric collection of dust from short-period comets. Meteorit. Planet. Sci. 37, 1491–1505.
Messenger, S., Keller, L.P., Stadermann, F.J., Walker, R.M., Zinner, E., 2003a. Samples of stars beyond the solar system: silicate grains in interplanetary dust. Science 300, 105–108.
Messenger, S., Stadermann, F.J., Floss, C., Nittler, L.R., Mukhopadhyay, S., 2003b. Isotopic signatures of presolar materials in interplanetary dust. Space Sci. Rev. 106, 155–172.
Messenger, S., Keller, L.P., Lauretta, D.S., 2005. Supernova olivine from cometary dust. Science 309, 737–741.
Messenger, S., Joswiak, D., Ito, M., Matrajt, G., Brownlee, D.E., 2009. Discovery of presolar SiC from comet Wild-2. Lunar Planet. Sci. Conf. XXXX, 1790.
Mikouchi, T., Tachikawa, O., Hagiya, K., Ohsumi, K., Suzuki, Y., Uesugi, K., Takeuchi, A., Zolensky, M.E., 2007. Mineralogy and crystallography of comet 81P/Wild 2 particles. Lunar Planet. Sci. Conf. XXXVIII, 1946.
Millar, T.J., Bennett, A., Herbst, E., 1989. Deuterium fractionation in dense interstellar clouds. Astrophys. J. 340, 906–920.
Mostefaoui, S., Hoppe, P., 2004. Discovery of abundant in situ silicate and spinel grains from red giant stars in a primitive meteorite. Astrophys. J. 613, L149–L152.
Mukhopadhyay, S., Nittler, L.R., 2003. D-rich water in interplanetary dust particles. Lunar Planet. Sci. Conf. XXXIV, 1941.
Mukhopadhyay, S., Nittler, L.R., Messenger, S., 2002. Hydrogen, carbon, and nitrogen isotopic imaging of cluster IDPs. Meteorit. Planet. Sci. 37, 104.
Nakamura, K., Messenger, S., Keller, L.P., 2005. TEM and NanoSIMS study of hydrated/anhydrous phase mixed IDPs: cometary or asteroidal origin? Lunar Planet. Sci. Conf. XXXVI, 1824.
Nakamura-Messenger, K., Messenger, S., Keller, L.P., Clemett, S.J., Zolensky, M.E., 2006. Organic globules in the Tagish Lake meteorite: remnants of the protosolar disk. Science 314, 1439–1442.
Nakamura-Messenger, K., Keller, L.P., Clemett, S.J., Jones, J.H., Palma, R.L., Pepin, R.O., Klöck, W., Zolensky, M.E., Messenger, S., 2008. New manganese silicide mineral phase in an interplanetary dust particle. Lunar Planet. Sci. Conf. XXXIX, 2103.
Nguyen, A.N., Stadermann, F.J., Zinner, E., Stroud, R.M., Alexander, C.M.O'D., Nittler, L.R., 2007. Characterization of presolar silicate and oxide grains in primitive carbonaceous chondrites. Astrophys. J. 656, 1223–1240.
Nittler, L., 1997. Presolar oxide grains in meteorites. AIP Conf. Proc. 402, 59–82.
Nittler, L.R., 2003. Presolar stardust in meteorites: recent advances and scientific frontiers. Earth Planet. Sci. Lett. 209, 259–273.
Nittler, L.R., Messenger, S., 1998. Hydrogen and nitrogen isotopic imaging of interplanetary dust. Lunar Planet. Sci. Conf. XXIX, 1380.
Nittler, L.R., Alexander, C.M.O'D., Gao, X., Walker, R.M., Zinner, E., 1997. Stellar sapphires: the properties and origins of presolar Al_2O_3 in meteorites. Astrophys. J. 483, 475–495.
Nittler, L.R., Alexander, C.M.O'D., Gallino, R., Hoppe, P., Nguyen, A.N., Stadermann, F.J., Zinner, E.K., 2008. Aluminum-, calcium- and titanium-rich oxide stardust in ordinary chondrite meteorites. Astrophys. J. 682, 1450–1478.
Palma, R.L., Pepin, R.O., Schlutter, D., 2005. Helium and neon isotopic compositions from IDPs of potentially cometary origin. Meteorit. Planet. Sci. 40, A120.
Quirico, E., Borg, J., Raynal, P.-I., Montagnac, G., d'Hendecourt, L., 2005. A micro-Raman survey of 10 IDPs and 6 carbonaceous chondrites. Planet. Space Sci. 53, 1443–1448.
Rietmeijer, F.J.M., 1985. A model for diagenesis in proto-planetary bodies. Nature 313, 293–294.
Rietmeijer, F.J.M., 1990. Salts in two chondritic porous interplanetary dust particles. Meteoritics 25, 209–213.
Rietmeijer, F.J.M., 2002. The earliest chemical dust evolution in the solar nebula. Chem. Erde 62, 1–45.
Rotundi, A., Baratta, G.A., Borg, J., Brucato, J.R., Busemann, H., Colangeli, L., d'Hendecourt, L., Djouadi, Z., Ferrini, G., Franchi, I.A., Fries, M., Grossemy, F., Keller, L.P., Mennella, V., Nakamura, K., Nittler, L.R., Palumbo, M.E., Sandford, S.A., Steele, A., Wopenka, B., 2008. Combined micro-Raman, micro-infrared, and field emission scanning electron microscope analyses of comet 81P/Wild 2 particles collected by Stardust. Meteorit. Planet. Sci. 43, 367–397.
Sandford, S.A., Aléon, J., Alexander, C.M.O'D., Araki, T., Bajt, S., Baratta, G.A., Borg, J., Bradley, J.P., Brownlee, D.E., Brucato, J.R., Burchell, M.J., Busemann, H., Butterworth, A., Clemett, S.J., Cody, G., Colangeli, L., Cooper, G., D'Hendecourt, L., Djouadi, Z., Dworkin, J.P., Ferrini, G., Fleckenstein, H., Flynn, G.J., Franchi, I.A., Fries, M., Gilles, M.K., Glavin, D.P., Gounelle, M., Grossemy, F., Jacobsen, C., Keller, L.P., Kilcoyne, A.L.D., Leitner, J., Matrajt, G., Meibom, A., Mennella, V., Mostefaoui, S., Nittler, L.R., Palumbo, M.E., Papanastassiou, D.A., Robert, F., Rotundi, A., Snead, C.J., Spencer, M.K., Stadermann, F.J., Steele, A., Stephan, T., Tsou, P., Tyliszczak, T., Westphal, A.J., Wirick, S., Wopenka, B., Yabuta, H., Zare, R.N., Zolensky, M.E., 2006. Organics captured from comet Wild 2 by the Stardust spacecraft. Science 314, 1720–1724.
Schulze, H., Kissel, J., Jessberger, E.K., 1997. Chemistry and Mineralogy of Comet Halley's Dust. ASP Conf. Series vol. 122, pp. 397–414.
Slodzian, G., Hillion, F., Stadermann, F.J., Zinner, E., 2004. QSA influences on isotopic ratio measurements. Appl. Surf. Sci. 231–232, 874–877.

Stadelmann, P.A., 1987. EMS—a software package for electron diffraction analysis and HREM image simulation in materials science. Ultramicroscopy 21, 131–145.
Stadermann, F.J., Floss, C., 2008. Abundance of presolar grains in comet Wild 2 and implications for transport and mixing in the solar nebula. Lunar Planet. Sci. Conf. XXXIX, 1889.
Stadermann, F.J., Floss, C., Gavinsky, A., Kearsley, A.T., Burchell, M.J., 2009. Calibrating the abundance determinations of presolar grains in Wild 2 cometary matter. Lunar Planet. Sci. Conf. XXXX, 1188.
Stern, S.A., 2003. The evolution of comets in the Oort cloud and Kuiper belt. Nature 424, 639–642.
Toppani, A., Robert, F., Libourel, G., de Donato, P., Barres, O., D'Hendecourt, L., Ghanbaja, J., 2005. A 'dry' condensation origin for circumstellar carbonates. Nature 437, 1121–1124.
Vollmer, C., Hoppe, P., Brenker, F.E., 2008. Si isotopic compositions of presolar silicate grains from red giant stars and supernovae. Astrophys. J. 684, 611–617.
Wooden, D.H., 2008. Cometary refractory grains: interstellar and nebular sources. Space Sci. Rev. 138, 75–108.
Wopenka, B., 1988. Raman observations of individual interplanetary dust particles. Earth Planet. Sci. Lett. 88, 221–231.
Yada, T., Floss, C., Stadermann, F.J., Zinner, E., Nakamura, T., Noguchi, T., Lea, A.S., 2008. Stardust in Antarctic micrometeorites. Meteorit. Planet. Sci. 43, 1287–1298.
Zega, T.J., Nittler, L.R., Busemann, H., Hoppe, P., Stroud, R.M., 2007. Coordinated isotopic and mineralogic analyses of planetary materials enabled by in situ lift-out with a focused ion beam scanning electron microscope. Meteorit. Planet. Sci. 42, 1373–1386.